Discovery of a Pulsating Component in a Decametric Frequency Range Suggesting a Rotating Super Black Hole at the Galactic Center as a Source

Tôhoku Geophys. Journ. (Sci. Rep. Tôhoku Univ., Ser. 5), Vol. 30, Nos. 2, 3 and 4, pp. 15-49, 1987

Discovery of a Pulsating Component in a Decametric Frequency Range Suggesting a Rotating Super Black Hole at the Galactic Center as a Source

HIROSHI OYA, MASAHIDE IIZIMA and AKIRA MORIOKA

(Received March 16, 1987)

Abstract: In a decametric frequency range from 25 MHz to 35 MHz, pulsating components with a period of 421.60 ± 0.01 msec have been discovered. The pulses are associated with an interpulse; the first pulse has a time width about 226 msec and the second pulse has a time width about 193 msec. The Fourier analyses of this pulse indicate a periodicity around 220 to 250 msec. From the observed direction and a large frequency dispersion corresponding to a distance ranging from about 9 kpc to 10 kpc, it is suggested that the decametric radiation with the pulsating component is coming from the center of our Galaxy. The power of pulses is estimated to be about 5×10^{34} erg/sec within 10 MHz bands. The source of the pulsating components which radiates extremely high energy is attributed to a rotating super black hole whose maximum mass is estimated to be about 6.5×10^{8} $M_\odot$ where $M_\odot$ is solar mass.

1. Introduction

Our galaxy is a well known source of nonthermal electromagnetic radiation in the decametric wavelength range. After the initial discovery by Jansky (1933; and 1935), many studies have been carried out on this radiation whose source regions are distributed throughout the Milky Way. It has been found (Reber, 1944; Moxon, 1946; Shain, 1953; Shain and Higgins, 1953; Higgins and Shain, 1954) that radio source is inhomogeneously distributed with a maximum intensity located at the center of the galaxy.

Recent studies of radio emissions from our galaxy have been gradually focused on the center especially in the high frequency range corresponding to cm wavelengths. The high level activity of the gas flow (Lacy *et al.*, 1979) within less than 1 pc of the center and the motion of the gas cloud emitting infrared radiation suggest the existence of a black hole at the galactic center (Lacy *et al.*, 1982). Lo and Claussen (1983), have identified ionized gas (plasma) flow at 6 cm wavelength using their very large array radio telescope. Within a range of 1000 AU around the galactic center, there are three plasma arms flowing into the central region. The flow of material besed on this observation is consistent with the energy release estimated from the infrared gas flow observations (Lacy *et al.*, 1979).

The purpose of the present paper is to report the discovery of pulsating components

Department of Geophysics and Astronomy II, Tohoku University, Sendai 980, Japan

of the decametric wavelength radiation whose source is most likely at the galactic center. It will be shown that these pulsating components may be emitted from layers very close to the surface of a super black hole at the galactic center. The limiting mass of the black hole is estimated to be 6.5×10^3 M$\odot$ where M$\odot$ is the solar mass which is considerably smaller than the previously inferred mass although the object is still a very large super black hole.

2. Observation System

2.1 *Principle*

Decametric radiations from the galaxy in a frequency range from 25 MHz to 33 MHz have been measured using three-stage super-heterodyne receivers. Detection of the pulsating components from the observed decametric radiations is however under very dificult conditions; the difficulties are due to broadening of the pulse widths associated with the large frequency dispersion as well as the multi-path or fluctuation of the propagation paths through galactic space over a distance of around 9 kpc to 10 kpc.

The well known frequency dispersion effect can be expressed for the delay time dT_D as

$$dT_D=-\left(\frac{L}{C}\right)\left(\frac{f_p}{f}\right)^2\left(\frac{df}{f}\right), \tag{1}$$

where f_p, f, L and c are the average plasma frequency in galactic space, the observation frequency, the distance of the source and the light velocity, respectively. In Fig. 1 and 2, the delay time dT_D versus the observation frequency for both the 30 Hz and the 60 Hz

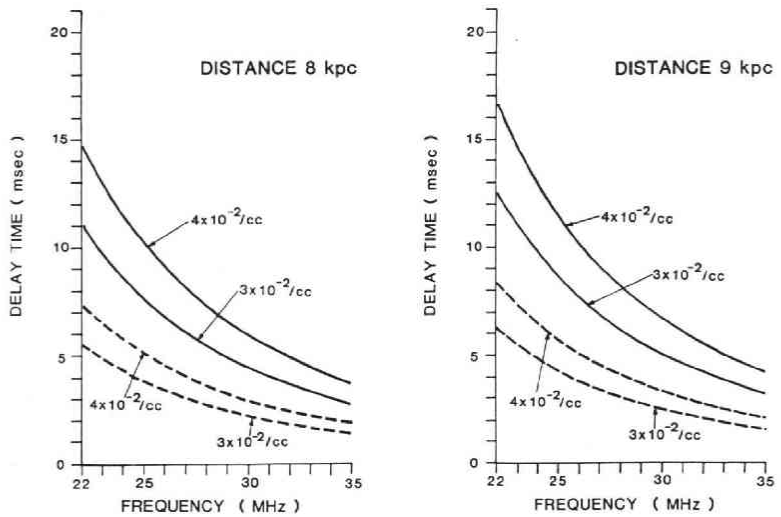

Fig. 1 Calculated delay times through galactic space with an electron number density of 4×10^{-2} and 3×10^{-2} for distances of 8 kpc and 9 kpc. The delay times dT_D are given versus observation frequencies for the frequency gap $df=60$ Hz (solid lines) and for the frequency gap $df=30$ Hz (dotted lines).

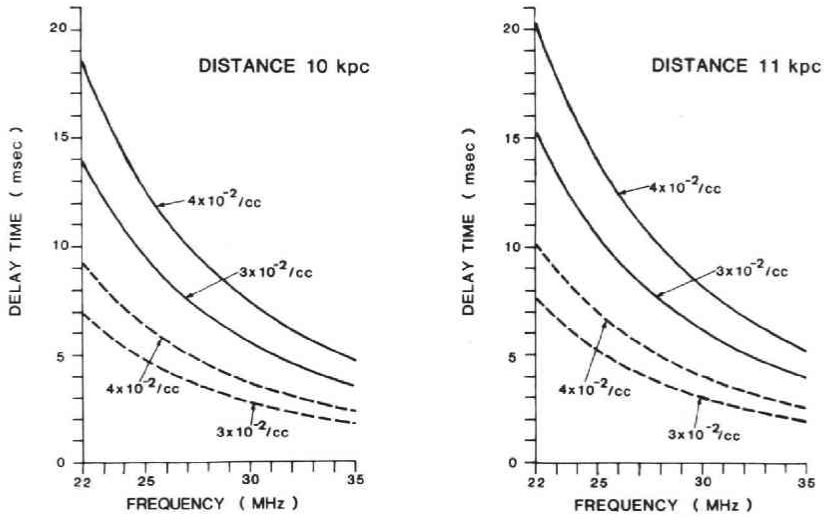

Fig. 2 Same with Fig. 1 for the distances of 10 kpc and 11 kpc.

frequency gap is given, for various distances from 8-11 kpc.

One of the most significant effects for broadening of the pulse width is the multi-path effects due to existing irregularities in the plasma through out galactic space. The estimation (see Appendix) gives that the averaged broadening of the pulse width dT_I can be expressed by

$$dT_I = \left(\frac{L}{c}\right) A \left(\frac{\Delta f_p}{f}\right)^4 \left(\frac{df}{f}\right)^2, \tag{2}$$

where A is a constant.

All of these broadening effects show that we are under a very serious disadvantage of the condition for the pulse detection when the observations are made in a low f value range such as the case of decametric radiation. However, when we select a small (df/f) value, i.e., a very narrow band, the problems are resolved. It is reported that dT_I which causes pulse-smearing exceeds 10 msec at 318 MHz (Hewish, private communication, 1985), for the dispersion $NL = (100\ \mathrm{cm}^{-3})\ pc$ where N and L are the electron number density and the distance respectively. In a frequency range less than 30 MHz, therefore, we should select a (df/f) value, less than 10^{-2} compared with the case of regular observations in the 300 MHz range. Considering this evidence, we have selected a very narrow band observation system.

Two kinds of observation systems have been employed. For observations during 1983 to 1985, we used an analog data handling system which is referred to in this report as system-A. After March 1986, the observations have been made using system-D which consists of a digital data handling system. Both of these receiving systems utilize a broad band Yagi antenna and a three stage super-heterodyne receiver with an especially narrow frequency band.

2.2 *System-A*

All of the data handling processes are made in analog stages in system-A. The band width df is set at 210 Hz by converting the observation frequency in the decametric frequency range down to a range from 220 Hz to 430 Hz. This 210 Hz band width in the analog system is devided into 7 channels. The signal from each channel with a 30 Hz band width is fed to the delay circuit so as to compensate for the dispersion effects given by eq (1).

When we investigate the emission from the source assumed to be near the galactic center, the estimated delay time for the arrival of pulses between two channels with a 30 Hz frequency gap is in a range from 2 to 4 msec for a frequency range from 25 MHz to 32 MHz (see Fig. 1). The total delay time for the arrival of the pulse for the 210 Hz band width is, therefore, in a range from 14 msec to 28 msec. By applying a delay compensation circuit, we can reconstruct the pulse height within this 210 Hz band width. In Fig. 3 and 4, the block diagrams of the observation and data analyses systems are given for system-A and system-D, respectively.

2.3 *System-D*

The data handling processes in system-D are made using the narrow band multi-channel divider, the A/D transform circuits and the computer aided delay compensation

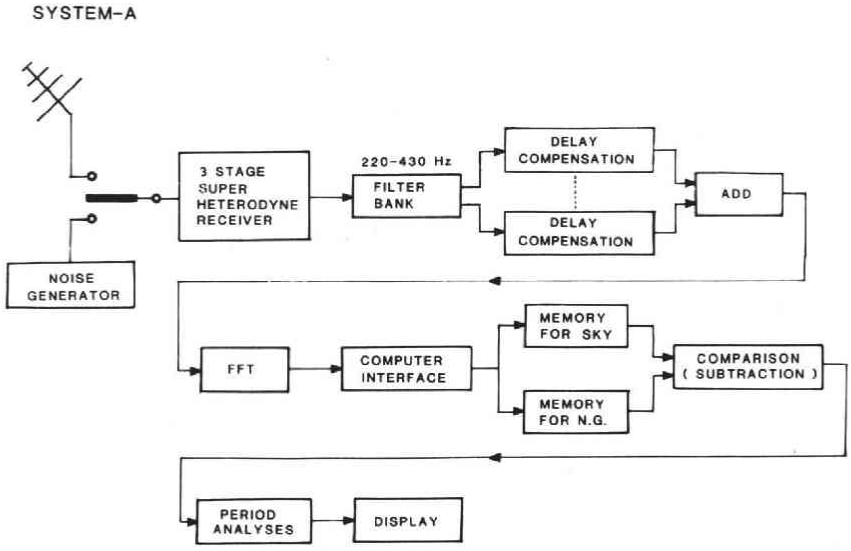

Fig. 3 Block diagram of the system A for observations and data analyses of decametric radiation from the galactic center. Passing through the 3 stage super heterodyne receiver, signals are fed into the filter bank where the signals in the frequency ranging from 220 Hz to 430 Hz are divided into 7 channels with the frequency gap of 30 Hz between neighboring channels. Delay compensation is made for each divided channel by applying the necessary delay to reconstruct the original pulses. After the delay compensation, the data analyses have been made using FFT and a computer system.

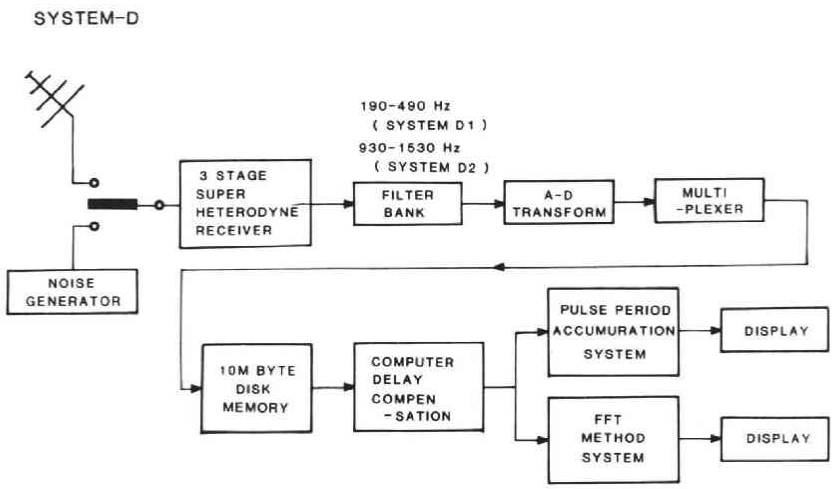

Fig. 4 Block diagram for system-D for observation and data analyses. The basic principle is same with System A but the digital computer is employed for the delay compensation system which consists of an A-D transformer, a Multiplexer, a 10 Mbite disk memory as well as computer delay compensation. This system D is applicable both for FFT analyses and pulse period accumulation methods. The filter banks used for the delay compensation consist of 10 channels with a frequency gap of 30 Hz for system D_1 and a frequency gap of 60 Hz for system D_2.

system. The dalay compensation is made through two different systems. The first is system-D_1, where the delay compensation is made up of a 210 Hz band width by having 7 channels of 30 Hz bandwidth each. Each channel in this delay compensation had an 8 Hz bandwidth. The second is the system-D_2 in which the delay compensation is made by dividing the 600 Hz band width into 10 channels with a 60 Hz frequency gap; signals from each channel are converted into a series of digital data from the analog to the digital converter. Samplings of one point datum (8 bits) are made every 0.5 msec and 4. 5 msec, respectively for system D_1 and for system D_2. The delay function for the compensation of the frequency dispersion is made using digital computer by shifting the relative addresses of the time serial data between different frequency channels.

3. Methods of Data Analyses

3.1 *Pulse period accumulation analyses*

Two data analyses techniques have been used; i.e. the first is the Fourier analyses to find hidden pulse periods, and the second is the method of the so called box-car averaging where the data $D(t)$ at time t_n ($n=1, 2, \ldots$) are overlapped with the data sampled at t_n+2mT_p in the following manner:

$$D(t_n)=\sum_{m=1}^{k} D(2mT_p+t_n), \tag{3}$$

where T_p is a given pulse period and k is the limit number of the sampling time m; t_n's

show the sample time within the 2 cycles of data. We call this method "pulse-period accumulation analyses". To confirm the existence of the pulse under a fairly large noise disturbance condition, it is necessary to check the symmetry of the obtained wave forms. Therefore we selected 2 cycles, i.e. $2T_p$ as the basic cycles for sampling of the data-points.

3.2 *Averaging Functions*

The total averaged times $k=14400$ in eq (3) was selected for the recent observations made in 1986; i.e. during the total period of 28800 T_p in eq (3). The sets of observation data of the galactic radio emissions have therefore been made continuously during 3 h 22 min, because $T_p=421$ msec. A large fluctuation of the pulse period due to the scintilation and multi-path effects of the rays through the Galactic space is thought to be dominant. Then, it is needed to find the averaged value of T_p. For the averaging purpose we used two methods; i.e. i) a multiple averaging method and ii) period tracking methods; both are explained in the following.

a) Multiple averaging method

The observed pulse period making fluctuation around the original pulse period given at the source. The concept of this fluctuation is depicted in panel (a) of Fig. 5. We have selected several periods from T_1 to T_n (see Fig. 5) around the expected original period at the source. The pulse forms $P(t, T_i)$ versus time t for the period Ti $(i=1\sim N)$ (obtained for each selected period T_i using eq (3)) are then finally averaged as

$$P(t, T_a)=\frac{1}{N}\sum_{m=1}^{N} P(t, T_m). \tag{4}$$

For the observations made by using system-D_2 in 1986, six cases of the period, i.e. $m=6$ in eq (4), from $T_{p1}=421{,}600$ msec to $T_{p6}=421.604$ msec are used; and finally the period is averaged by using eq (4) giving $T_a=421.602$ msec, as will be given in the nest section.

b) Period-Tracking Method

This is the method to make tracking the variation of the fluctuating period. For this purpose, the intervals for the box-car averaging period are made shorter than the case of the multiple averaging method by dividing the total interval into several segments of sub-periods, as the concept has been illustrated in panel (b) of Fig. 5.

In this method, the average value is obtained by superposing the pulse forms obtained in sub-accumulation-periods, so as to keep the obtained pulse train symetrical as possible; i.e.,

$$P(t_n, T_a)=\frac{1}{N}\sum_{i=1}^{N} P(t_n+T_i, T_{si}), \tag{5}$$

where T_{si} is a period found in the i-th sub-accumulation-period and T_i is the adjusted time period introduced for each sub-sccumulation-period so as to make optimum choice for the superpositon of pulse forms obtained in sub-accumulation-periods.

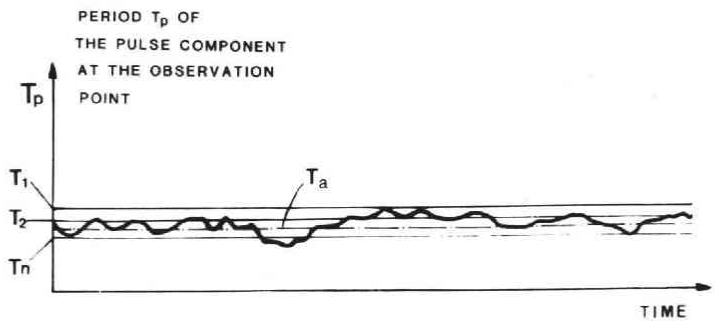

(a) MULTIPLE AVERAGING METHOD

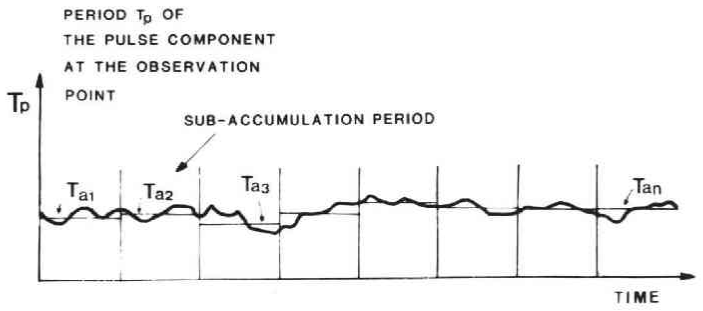

(b) PERIOD TRACKING METHOD

Fig. 5 Schematic illustrations of averaging times for the multiple averaging method (a) and Period tracking method (b). The actual observation period of the pulse is making fluctuation with the period given by the thick solid curve around the average value T_a due to the long distance propagation through galactic space. The analyses of the multiple averaging method (a) is then made by selecting difering multiple periods from T_1 to T_n; to obtain the final results, data are averaged for the cases corresponding from T_1 to T_n. In the period tracking method (b), the pulse forms are obtained by dividing the total observation periods into the segments of the sub-period. Tracking of the pulse period is made in each sub-period as T_{a1}, T_{a2}, ···, T_{an}. The wave forms in sub-periods are averaged to obtain the final results.

4. Observations and Identification of the Pulse

4.1 *Observation Periods*

Observations have been made from May 1983 to July 1986, mainly in the periods of spring and summer when the Galactic center was observable in the post midnight time when ionospheric electron density was sufficuently reduced to values to avoid the interference from broadcast waves (Oya *et al.*, 1983).

Observations during 1983 and 1984 were devoted to the search for the pulsating components using the Fourier analyses methods. The receiving system-A had been developed and established during this periods. More accurate and confidential methods

Table 1. Observation Periods and Systems

Year	Month/Day	Frequency (MHz)	Observation system	Comments on data analyses
1983	5/3, 9	29.4	A	Analog spectrum analyses using auto-correlator. (Play back VTR data)
	8/23, 29	29.5	A	
1984	4/5-7	23.9-29.9	A	Analog spectrum analyses using auto-correlator. (Play back Data Recorder)
	5/1, 2	24.75-35.2	A	
1985	4/30-5/3	24.5-31.8	A	Analog spectrum analyses using FFT.
	6/22	26.8-29.7	A	
	7/1-6	25.5-32.4	A, D_1	Aonalog and digital spectrum analyses using FFT; Pulse period accumulation analyses (Period tracking method)
1986	5/10, 13, 14	25.5, 29.3	D_2	Analog and digital spectrum analyses using FFT; Pulse period accumulation analyses. (Multiple averaging method)
	5/20, 21, 24, 28	26.2, 27.7, 29.9, 32.2	D_2	
	6/3, 4, 8	29.4, 29.9, 32.1	D_2	
	6/10, 11, 17	30.6, 31.2, 31.4	D_2	
	6/21, 24, 25	27.7, 29.3	D_2	
	6/28, 29, 7/1, 2	25.5, 28.4, 31.4	D_2	
	7/5, 9, 15, 16	26.3, 30.6	D_2	
	7/30, 31, 8/2,	26,3, 29.3	D_2	

A : SYSTEM-A, D_1 : SYSTEM-D_1, D_2 : SYSTEM-D_2

of data analyses were introduced for the data reduction in 1985 and 1986. The observation intervals are indicated in Table 1.

To confirm the existence of the pulse component, the pulse-period accumulation method (see Sec. 3 and eq (3)) was applied for the data observed in 1985 and 1986.

4.2 *Results of Period-Tracking Method for the data in 1985*

The observation data in 1985 were obtained by system-D_1 employing the period-tracking method. The pulse period T_p was determined in a range from 421.58 to 421.71 msec for the pulses at 25.5 MHz and also found in a range from 421.58 msec to 421.90 msec for the pulses at 29.3 MHz. In Fig. 6, the observation data for the period when the antenna was directed to the Galactic center (Panel 1) and the observations in the case of absence of the Galactic center (Panel b) are indicated for $f=25.5$ MHz. In both cases, the data were averaged by applying the pulse-period accumulation analyses 400 times ($k=400$) in each sub-accumulation-period data. In this case, accumulation was again made by setting the basic interval to twice the cycle ($2T_p$) of the expected pulse period T_p. The pulse forms were obtained here for each 340 sec data-set sweeping the assumed

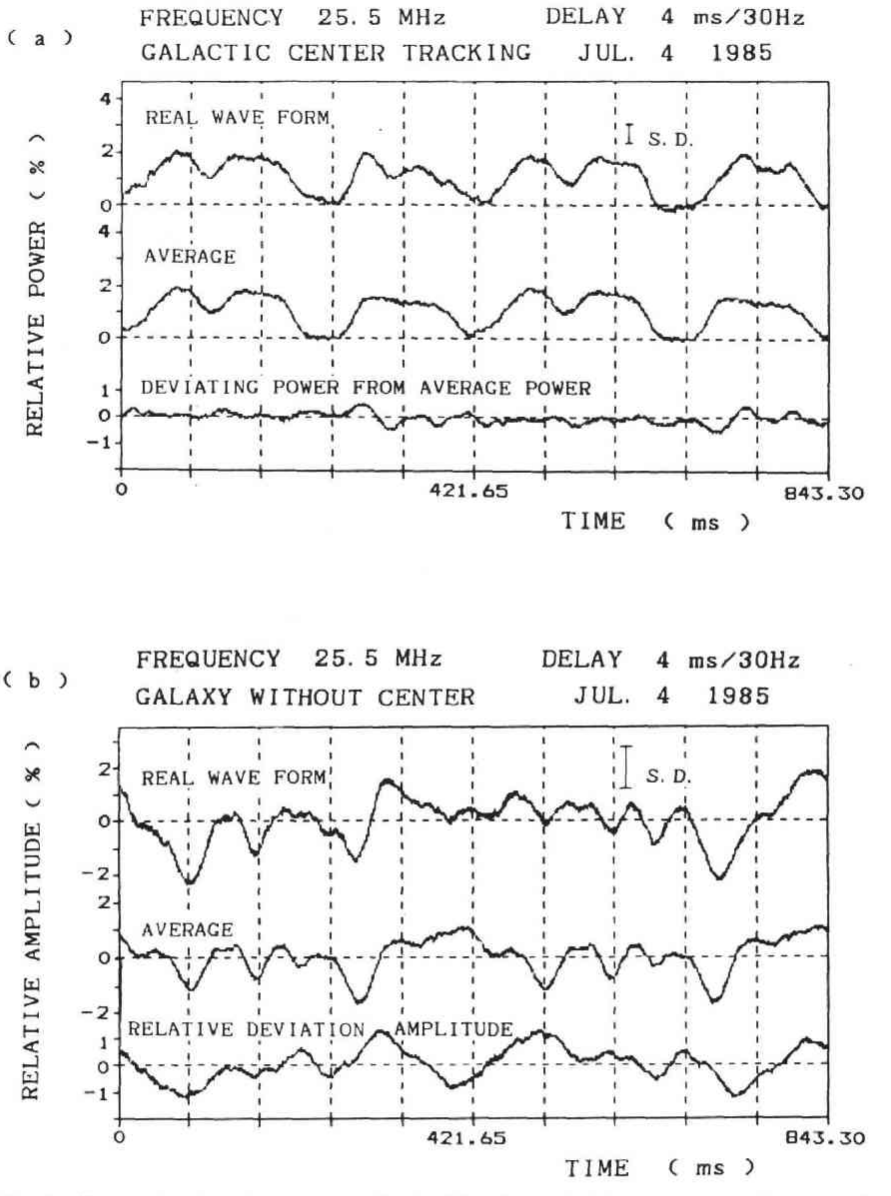

Fig. 6 Observed pulses at 25.5 MHz obtained by the period tracking method averaged over 340 sec for the signal coming from the direction of the galactic center (a) and also for the galactic decametric waves when the galactic center is not observable (b). Observations were mad on July 4, 1985 using system D_1. The final data (real wave form), the averaged wave form for two cycles (average) and the deviation of power from the average (relative deviation amplitude) are indicated from top to bottom in each panel. S.D. shows the standard deviation. The time interval from the left end to the right end of the abscissa is $2T_p$ (=843.48 msec). It is noted that the pulse (panel a) consists of two sub-pulses which show asymetry with the pulse width of 0.54 T_p for one sub-pulse and the pulse width of 0.46 T_p for the other sub-pulse. No pulse form can be identified when the galactic center is below the horizon (panel b).

period T_p for 421.0 to 427.9 msec; and the period from 421.58 to 421.90 msec were determined as a suitable range for the pulse period T_p for the sub-accumulation-period with $k=400$. Then four succeeding pulse forms in sub-accumulation-periods were averaged. That is, 1600 times of the $2T_p$ period (2 cycle) were averaged using eq (5), with $N=4$.

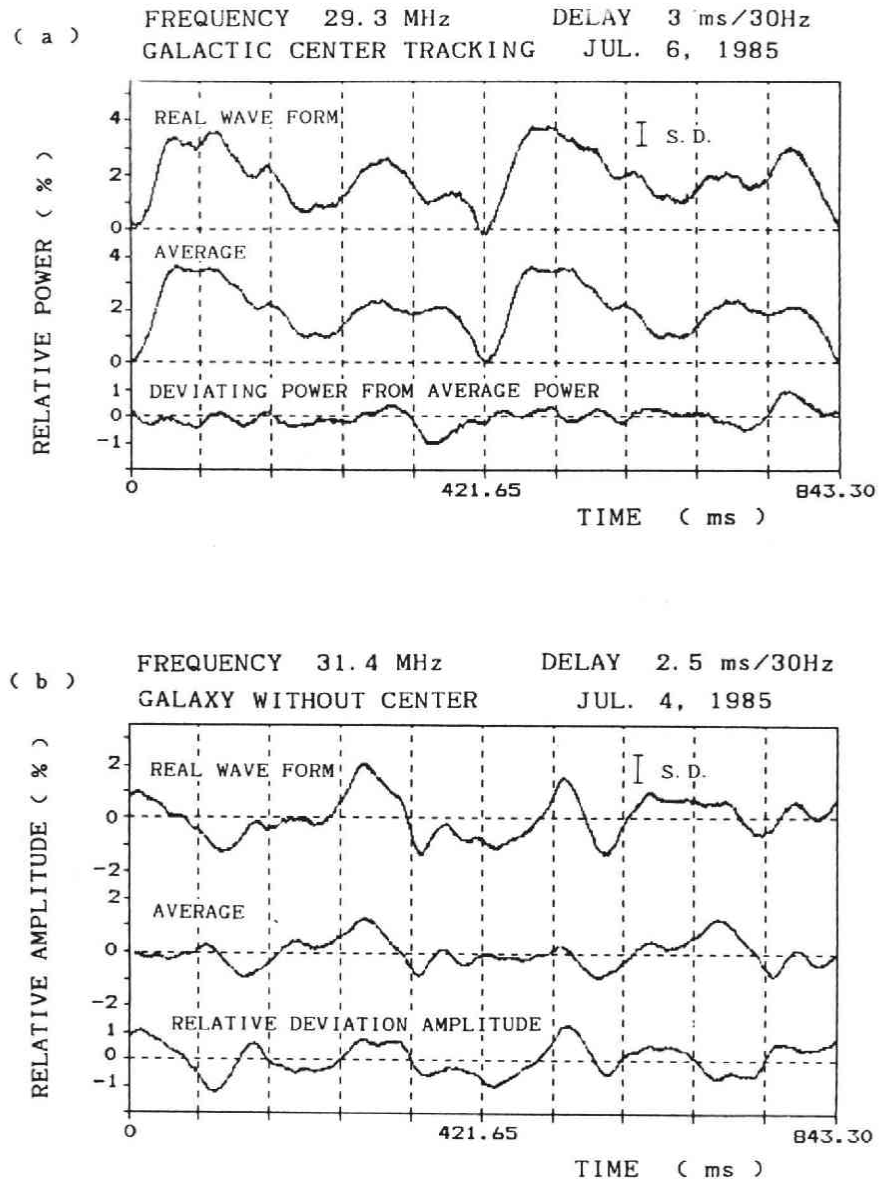

Fig. 7 Same with Fig. 6, for the observations made on July 6, 1985 at a frequency of 29.3 MHz (a) and for the case of no galactic center at a frequency of 31.4 MHz (b) observed on July 4, 1985.

Clear pulse trains which consists of two sub-pulses with asymetrical pulse widths have been identified. That is, the first pulse occupies 54% of the pulse period T_p including associated dip intervals while the second pulse occupies the pulse width about 46% of the pulse period T_p again including the associated dip intervals. It was confirmed that this pulse form cannot be observed at all, for the case where no Galactic center is observable within the view angle of the antenna.

In Figure 7, the results of the obtained pulse form applying the pulse-period accumulation analyses for 29.3 MHz data are given. The results are compared with that for the signal from the noise generator which is applied to the same receiving and data analyses systems (panel b). Thus, it is confirmed that no pulse is existing for the case of noise generator, while there is, again, an apparent pulse train in the observation data from the galactic center. The pulse again consists of two pulse components whose pulse widths show asymetrical feature as 54% and 46% of the total period T_p, respectively for the first and second pulses.

4.3 *Results of Multiple Period Averaging Method for the Data in 1986.*

The existence of the 421.60 msec pulse is further comfirmed for the data observed in 1986 (see table 1). Analyses were made using both of the system-D_1 and system-D_2. The set-up of system-D_2 is newly constructed and is independent to the set-up for system-A and system D_1. We can, therefore, make further confirmation that the existence of the pulse is not an instrumental effect.

Improvement has also been made by extending the interval of observation periods over 3 h 22 min for one data set (only 8 minutes for observations made in 1985). Typical examples of the pulse forms obtained at 26.3 MHz and 29.3 MHz are indicated in Figs. 8 and 9. In panel (a) of each figure, green curves indicate the results of the pulse forms for $2T_p$ obtained by the pulse period accumulation analyses and red curves show the average wave forms of these two cycle data. Though there are remaining in the pulse forms the noise disturbances (given in black curves) which are given by deviation of green curves from the red curves, the data show clear pulse trains which consists of two sub-pulses that occupy 56% of T_p for the first pulse and occupy 44% of T_p for the second pulse, again including assoiciated dip intervals. These features of the sub-pulses are also consistent with the results observed in 1985 at 25.5 MHz and 29.3 MHz ($0.54\,T_p$ for the first pulse width and $0.46\ T_p$ for the second pulse width).

Because data are now available in longer time intervals than the observations in 1985, (3 h 22 mins in 1986, and 8 minutes for 1985 data), we can determine the period more accurately than the results in 1985. That is, the period is determined in a range from 421.600 to 421.604 msec.

As has been indicated in panels (c) of Figs. 8 and 9, for the results of data analyses observed at 26.3 and 29.3 MHz, respectively, no pulse components could be identified when the Galactic center was absent from the field of view of the antenna. It was also confirmed that the pulses were not generated by the observation instrument or system, as we can clearly see in the data given in Fig. 8 of panel (b), where the analyses have been

(a)

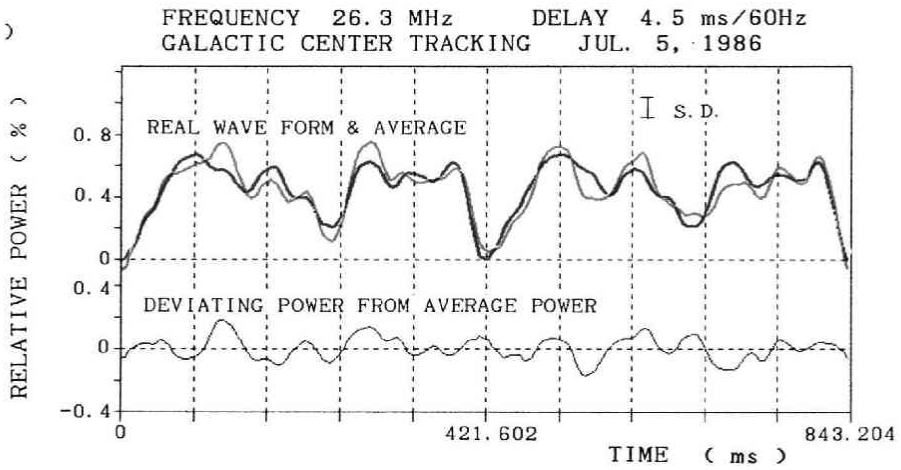
FREQUENCY 26.3 MHz DELAY 4.5 ms/60Hz
GALACTIC CENTER TRACKING JUL. 5, 1986
REAL WAVE FORM & AVERAGE
S.D.
DEVIATING POWER FROM AVERAGE POWER
RELATIVE POWER (%)
0.8
0.4
0
0.4
0
-0.4
0
421.602
843.204
TIME (ms)

(b)

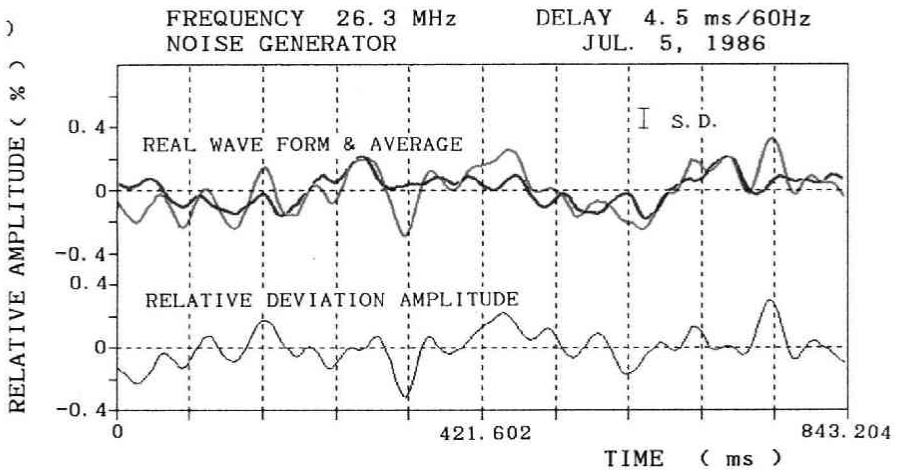
FREQUENCY 26.3 MHz DELAY 4.5 ms/60Hz
NOISE GENERATOR JUL. 5, 1986
REAL WAVE FORM & AVERAGE
S.D.
RELATIVE DEVIATION AMPLITUDE
RELATIVE AMPLITUDE (%)
0.4
0
-0.4
0.4
0
-0.4
0
421.602
843.204
TIME (ms)

(c)

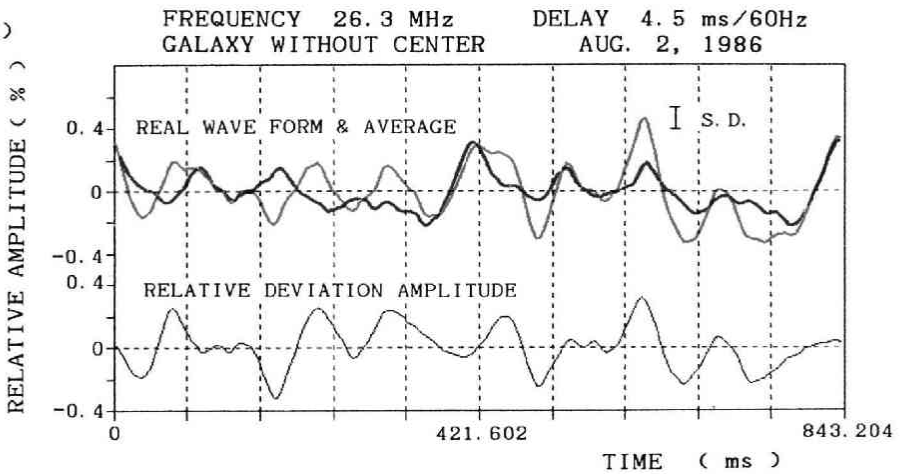
FREQUENCY 26.3 MHz DELAY 4.5 ms/60Hz
GALAXY WITHOUT CENTER AUG. 2, 1986
REAL WAVE FORM & AVERAGE
S.D.
RELATIVE DEVIATION AMPLITUDE
RELATIVE AMPLITUDE (%)
0.4
0
-0.4
0.4
0
-0.4
0
421.602
843.204
TIME (ms)

made using the exact same methods for the signal from the noise generators.

5. Comparison with the result of Fourier Analyses

All of the observations made in 1984, and a fairly large part of the observations made in 1985 have been made by applying Fourier transform analyses only, without using the method of the pulse period accumulation analyses. The results show that the remarkable spectral features are enhanced near the 200–250 msec period, i.e. at the frequency of 4 Hz$\pm$0.5 Hz and its harmonics, as has been given in Fig. 10.

There seems to be a discrepancy when comparing the results of the pulse period accumulation method which revealed the period of 421.60 msec with the sub-pulses with the time width of 234–250 msec for the first pulse and 187–200 msec for the second pulse. An investigation to solve this discrepancy has been made by taking the Fourier transformation for the pulse form obtained by the pulse period accumulation analyses. As has been given in Fig. 11, the spectra obtained by the Fourier transform method show the characteristic frequency near 4 and 5 Hz; and also higher harmonics near 8 and 9 Hz with a low peak around 2 and 3 Hz.

Further confirmation has been made by analytical methods applied to the model pulse given in Fig. 12 (a). The analysed spectra $G(\omega)$ using equation

$$G(\omega)=\left|\frac{1}{2T_o}\int_{-T_o}^{T_o} P(t)\,e^{-i\omega t}\,dt\right|, \tag{6}$$

is given in Fig. 12 (b) where T_o is an interval used for Fourier analyses, and $p(t)$ is the function given in Fig. 12 (a). We can see in this figure a remarkable coincidence between the actual observations and the model analyses. This coincidence shows that the basic period 421 msec is hidden or toned down due to existing sub-pulses when we apply the Fourier transformation analyses. Considering the results of these studies, we can conclude that the results of observations applying Fourier analyses, made in 1984 and 1985, are completely consistent with that of the pulse-period accumulation analyses.

Concentrating on the spectum level of the 250 msec period in the data of the Fourier analyses method obtained in 1985, we can then add further information concerning the characteristics of the pulse-component from the Galaxy.

In Fig. 13, the directivity is given for the observation at three frequencies, such as 28.4, 31.4, and 32.5 MHz, again using the results of the Fourier transformation method

Fig. 8 Typical observation rerults of the pulses from the galactic center observed by using System-D_2 on July 5, 1986 at frequency 26.3 MHz (a) with the results for noise generator (b) and for the case of no galactic center (c, on August 2, 1986). The green and red curves show the resultant wave form and the averaged wave form for two cycle data, respectively. S.D. shows the standard deviation. Deviations of the green curve data from the corresponding red curve data are indicated by black curves which are the corresponding disturbance levels of the background noises. The pulses with the period of 421.602 msec consist of the two sub-pulses (panel a). No Pulses can be identified for the case of the observation for the noise generator (b) and for the case of galactic emissions when the galactic center is under the horizon (Panel c). The delay compensation for all of these cases is adjusted to 4.5 m sec/60 Hz.

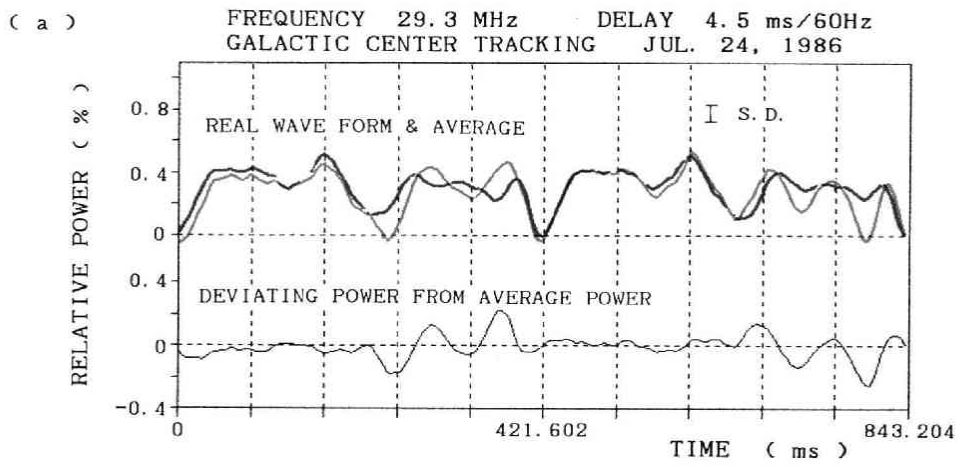
(a)
FREQUENCY 29.3 MHz DELAY 4.5 ms/60Hz
GALACTIC CENTER TRACKING JUL. 24, 1986
RELATIVE POWER (%)
0.8
0.4
0
0.4
0
-0.4
REAL WAVE FORM & AVERAGE
I S.D.
DEVIATING POWER FROM AVERAGE POWER
0
421.602
843.204
TIME (ms)

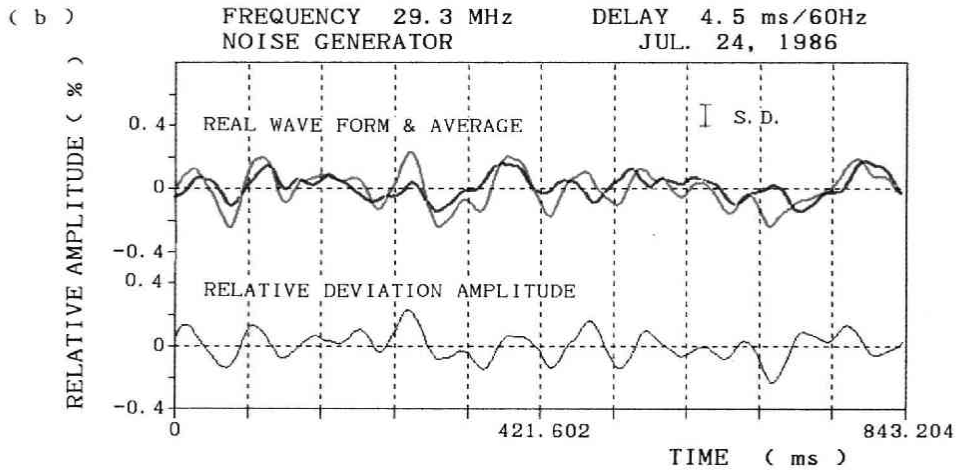
(b)
FREQUENCY 29.3 MHz DELAY 4.5 ms/60Hz
NOISE GENERATOR JUL. 24, 1986
RELATIVE AMPLITUDE (%)
0.4
0
-0.4
0.4
0
-0.4
REAL WAVE FORM & AVERAGE
I S.D.
RELATIVE DEVIATION AMPLITUDE
0
421.602
843.204
TIME (ms)

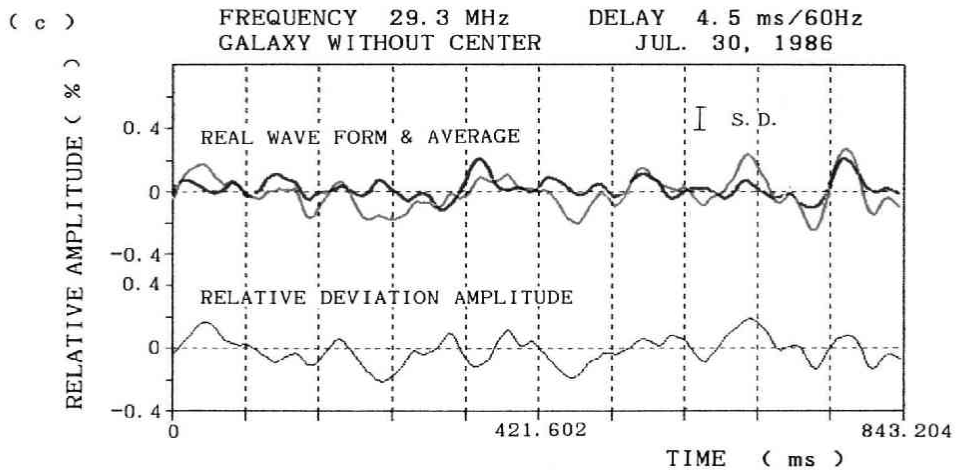
(c)
FREQUENCY 29.3 MHz DELAY 4.5 ms/60Hz
GALAXY WITHOUT CENTER JUL. 30, 1986
RELATIVE AMPLITUDE (%)
0.4
0
-0.4
0.4
0
-0.4
REAL WAVE FORM & AVERAGE
I S.D.
RELATIVE DEVIATION AMPLITUDE
0
421.602
843.204
TIME (ms)

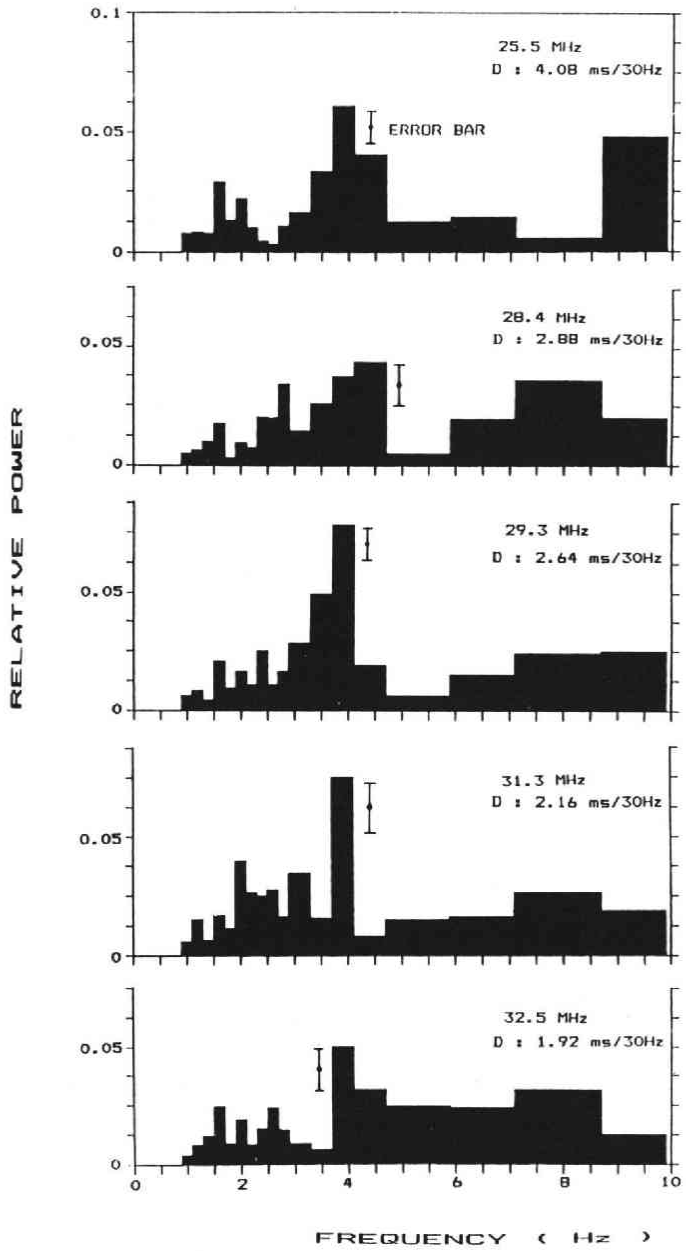

Fig. 10 Results of the Fourier analyses for the observations made on July 2, 1985 for the case where the antenna is directed to the galactic center, at frequencies of 25.5, 28.4, 29.3, 31.3 and 32.5 MHz. The spectra are indicated by subtracting the component of random noises. FFT analyses have been made after making delay compensations at the best delay compensation time whose values are given by D's in each panel.

Fig. 9 The format is basically the same as Fig. 8 for the case of the observation at 29.3 MHz made on June 24, 1986. Panels (a) (b) and (c), show, respectively, the results for the galactic center, the noise generator and the galactic emissions when the galactic center is under the horizon.

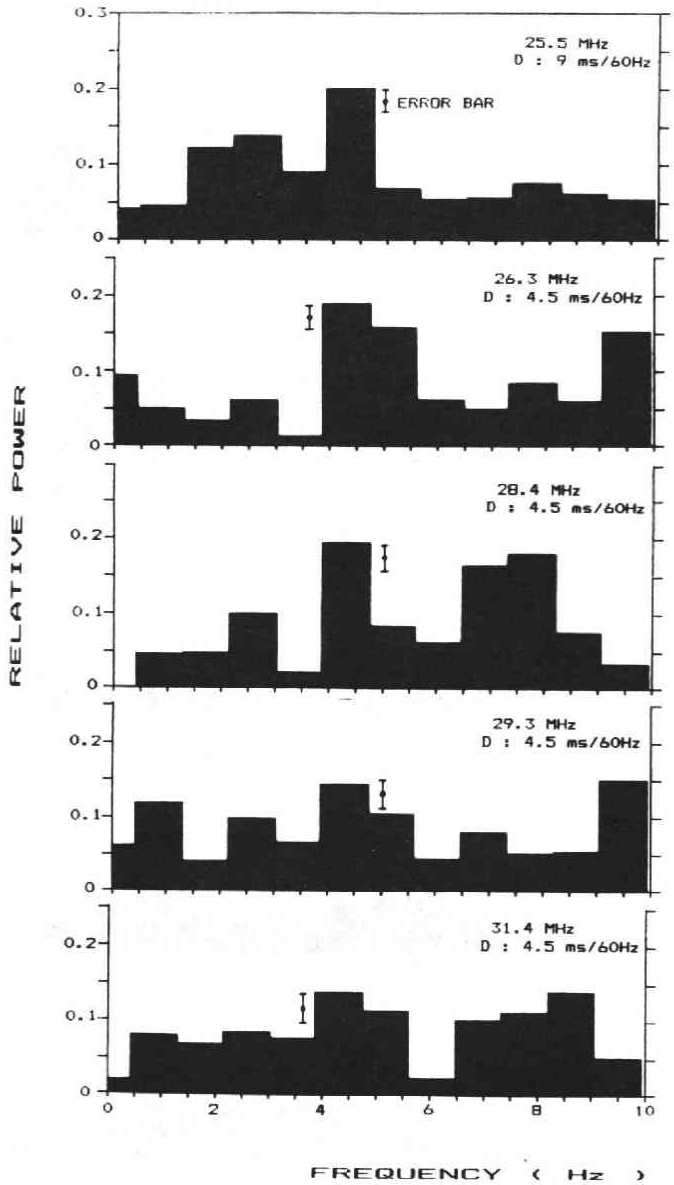

Fig. 11 Results of FFT analyses for the pulses obtained by the pulse period accumulation method at 25.5 MHz (corresponding to panel a of Fig. 15), 26.3 MHz (corresponding to panel b of Fig. 15), 28.4 MHz (corresponding to panel c of Fig. 15), 29.3 MHz (corresponding to panel a of Fig. 16), 31.4 MHz (corresponding to panel b of Fig. 16).
It is remarkable that the peaks of the spectra are indicated at 4 and 5 Hz ; and small sub-peaks near 2.5 Hz.

picking up the component of 220-250 msec periods. The results show that the source is located in the direction of the Galactic center within an accuracy of the directivity of the dipole antenna.

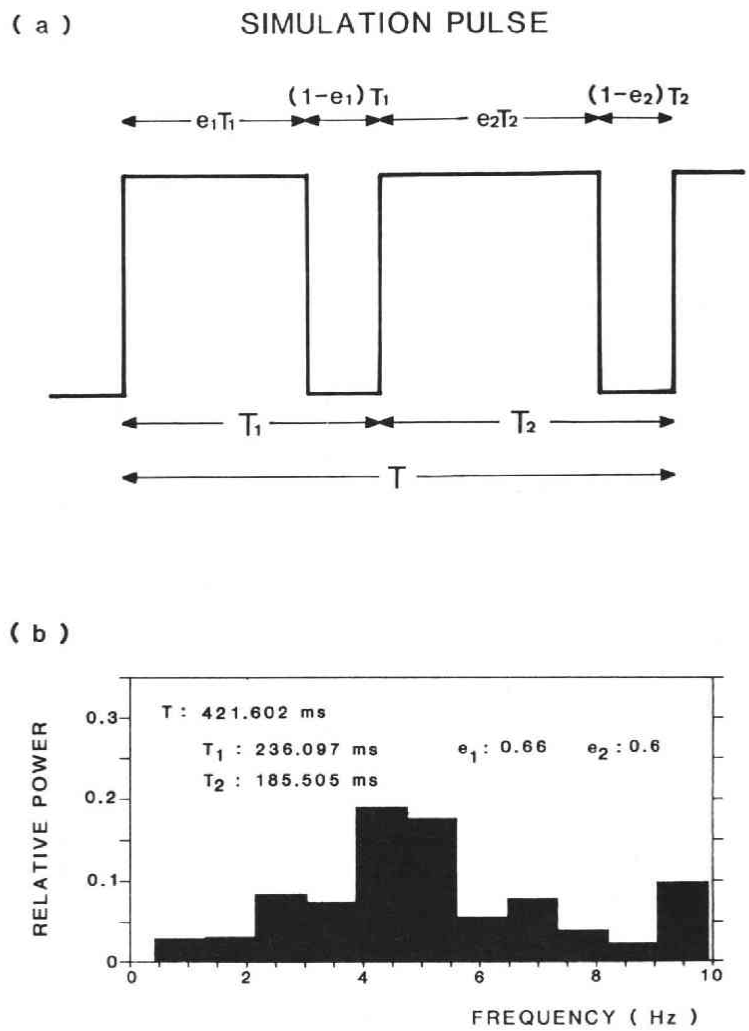

Fig. 12 Simulation pulse form to represent observed pulses from the Galactic center (a) and the Fourier transform of this wave form (b). Complete coincidence of the spectra forms in Figs. 10, and 11 with the spectrum in Fig. 12 (b) shows that the FFT results obtained in 1985 correspond to the pulse form which is revealed by the pulse period accumulation method (results are displayed in Figs. 8 (a), 9 (a), 15 and 16).

For the case of the Fourier analyses method, observations have been made using system-A where the delay compensations have been made through analog delay circuits. In Fig. 14, the power of the 250 msec period component has been plotted as the function of the dispersion time for the five frequencies. The results show that the 250 msec period component becomes apparent for the dispersion time expected for the source with $NL=320$ pc/cm^3, where N is the electron number density and L is the distance, as has been indicated by white arrows. These results give additional confirmation to the results of the pulse-period accumulation analyses as will be given in the next section.

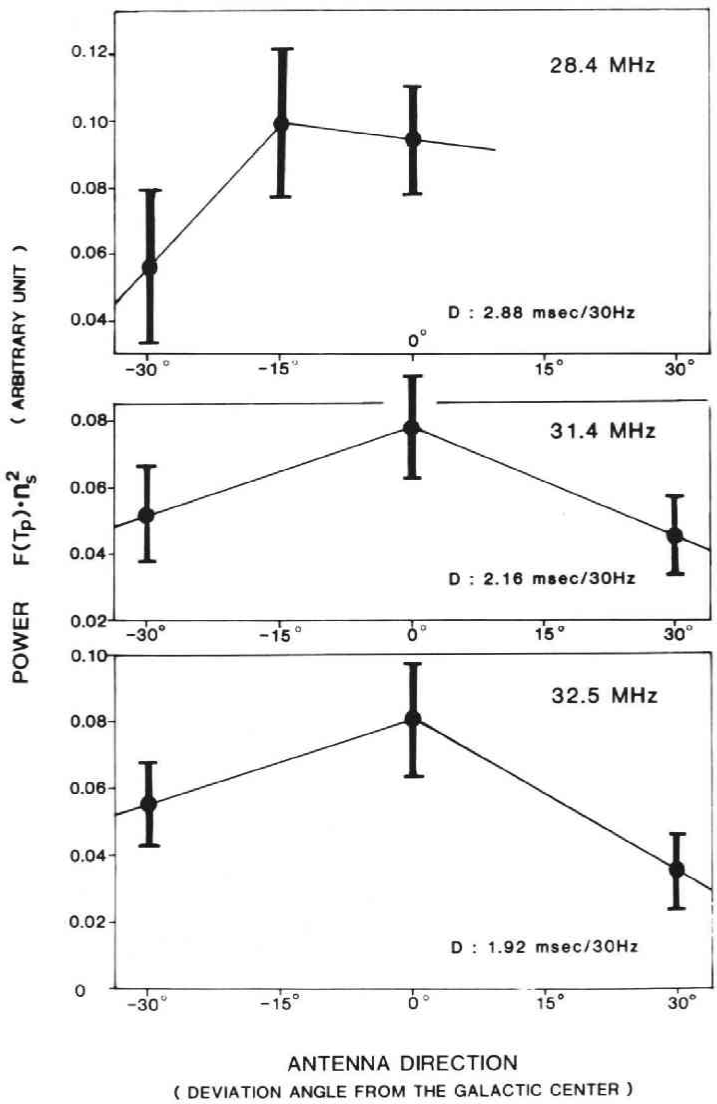

Fig. 13 Peak power of the spectra near 4 Hz, versus the antenna deviation angle measured from the direction of the galactic center. Measurements had been made at frequencies 28.4, 31.4 and 32.5 MHz ; the delay compensation time D is adjusted to 320 pc/cm^3, corresponding to 9 kpc for $N=0.03$/cc at each observation frequency.

6. Characteristics of the Decametric Pulse

a) Frequency range

The pulse form determined by applying the multiple average method of the pulse-period accumulation analyses over the period range from 421.600 to 421.604 msec are displayed in Fig. 15 (for frequencies 25.5, 26.3, and 28.4 MHz) and in Fig. 16 (for 29.3 and 31.4 MHz). The asymetry between two sub-pulse widths is consistently observed in all

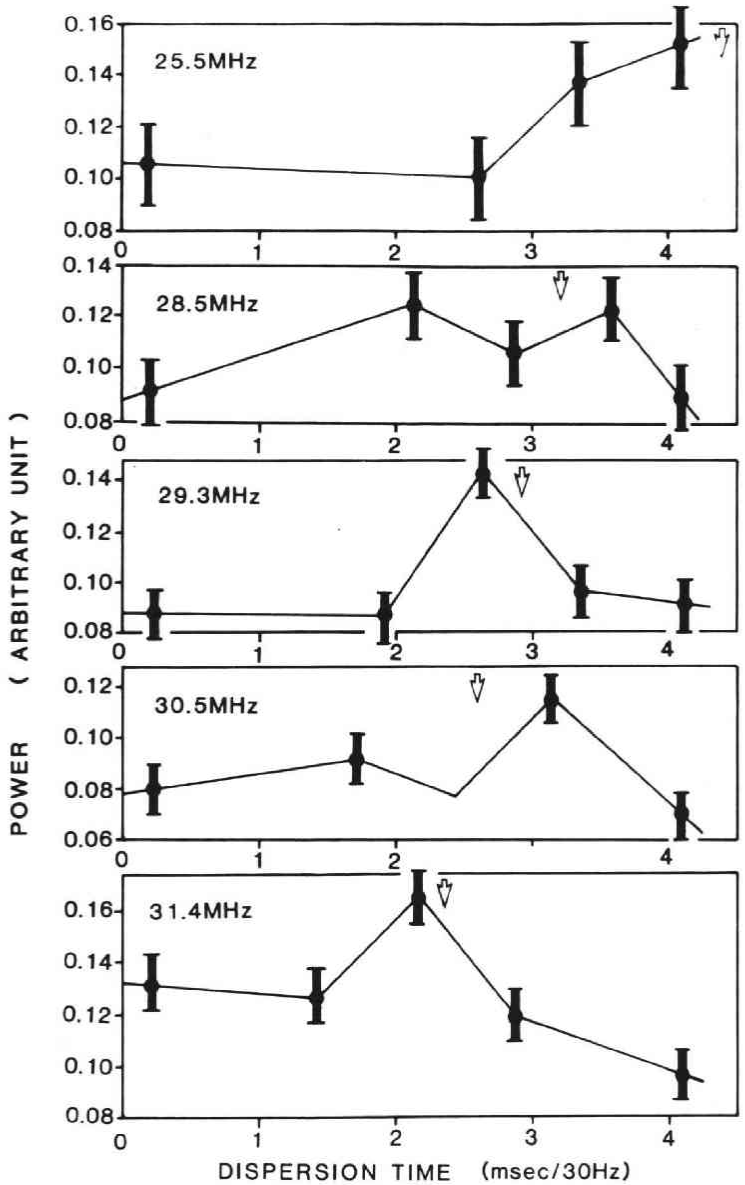

Fig. 14 Peak power level of the Fourier spectra near 4 Hz, corresponding to the 422 msec pulse, versus the dispersion compensation time (called dispersion time hear) in the unit of m sec/30 Hz. The arrow in each panel shows the estimated best fit compensation time (or dispersion time) corresponding to 320 pc/cc which indicates the source distance at about 9 kpc for the galactic plasma number density of 0.03/cc. The results show that the pulse source is located at a distance of about 9 kpc.

of the frequency ranges. By correcting frequency dependency of the antenna gain in this frequency range, the intensity characteristics versus frequency of the pulse component have been obtained as given in Fig. 17.

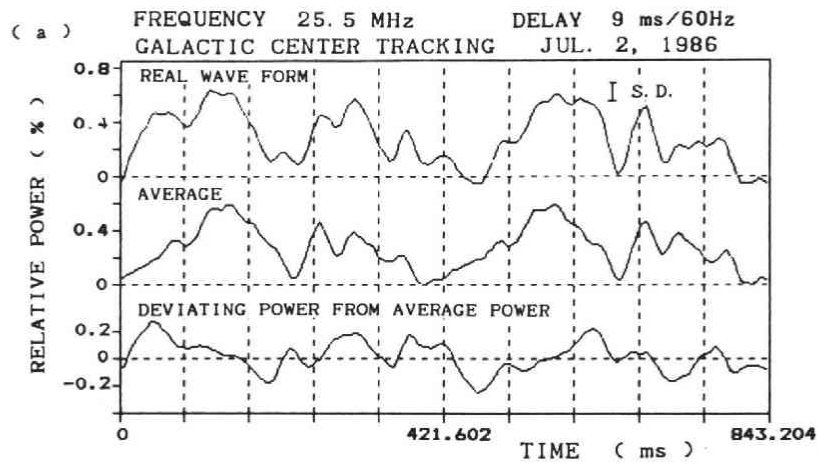
(a)
FREQUENCY 25.5 MHz
DELAY 9 ms/60Hz
GALACTIC CENTER TRACKING
JUL. 2, 1986
REAL WAVE FORM
I S.D.
AVERAGE
DEVIATING POWER FROM AVERAGE POWER
RELATIVE POWER (%)
0.8
0.4
0
0.4
0
0.2
0
-0.2
0
421.602
843.204
TIME (ms)

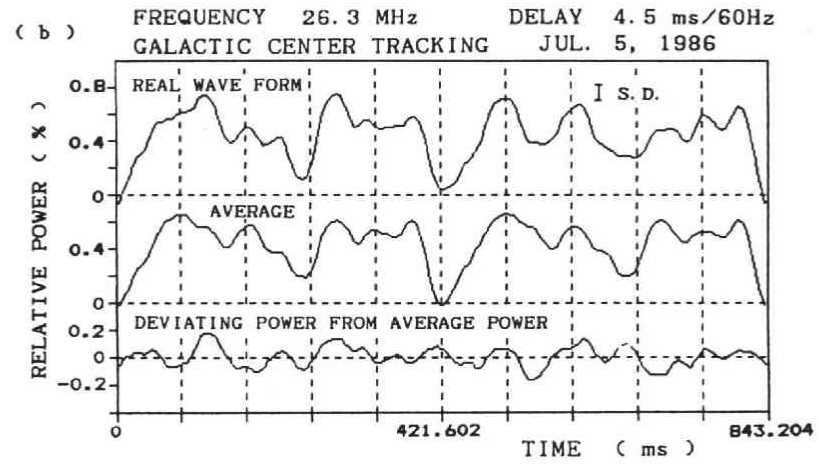
(b)
FREQUENCY 26.3 MHz
DELAY 4.5 ms/60Hz
GALACTIC CENTER TRACKING
JUL. 5, 1986
REAL WAVE FORM
I S.D.
AVERAGE
DEVIATING POWER FROM AVERAGE POWER
RELATIVE POWER (%)
0.8
0.4
0
0.4
0
0.2
0
-0.2
0
421.602
843.204
TIME (ms)

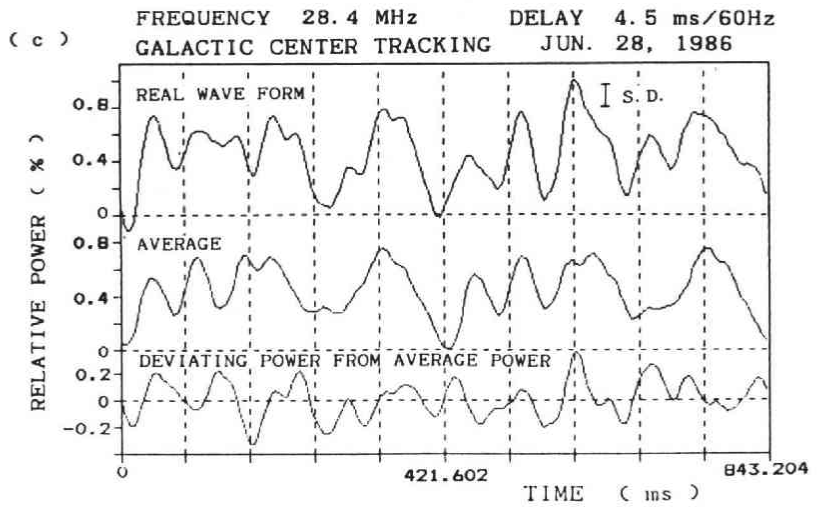
(c)
FREQUENCY 28.4 MHz
DELAY 4.5 ms/60Hz
GALACTIC CENTER TRACKING
JUN. 28, 1986
REAL WAVE FORM
I S.D.
AVERAGE
DEVIATING POWER FROM AVERAGE POWER
RELATIVE POWER (%)
0.8
0.4
0
0.8
0.4
0
0.2
0
-0.2
0
421.602
843.204
TIME (ms)

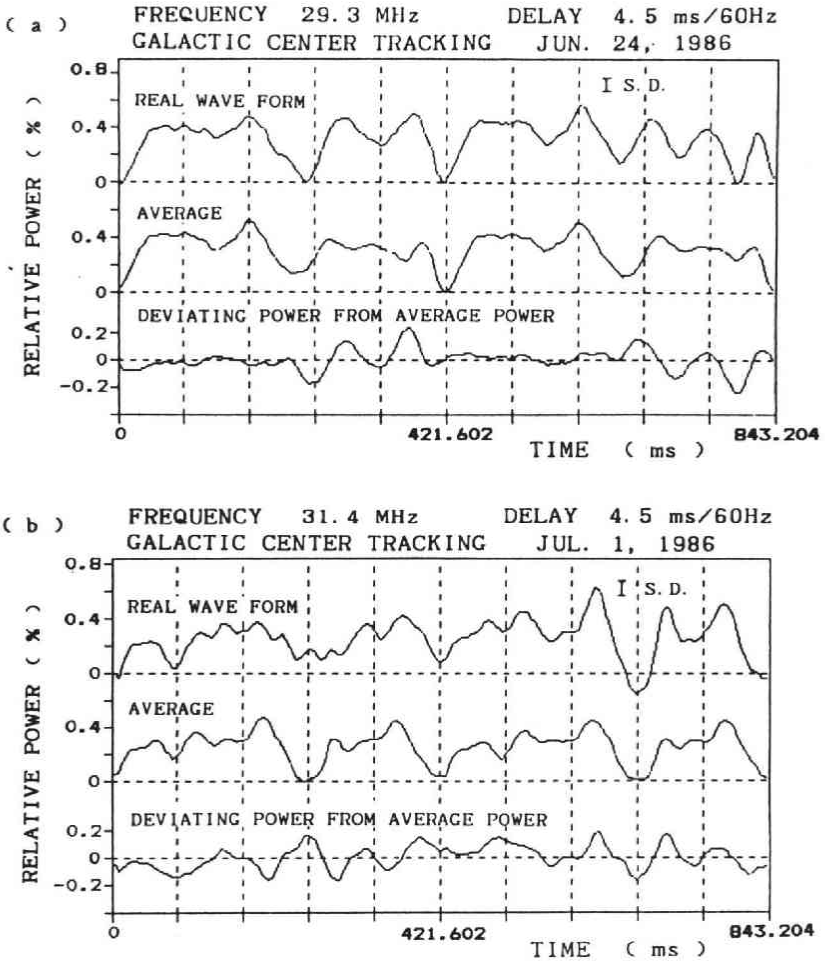

Fig. 16 Same with Fig. 15 for a frequency of 29.3 MHz observed on June 24, 1986 (a) and for 31.4 MHz observed on July 1, 1986 (b).

b) Delay effects

In the system-D_2, the delay compensation (see Sec. 2) has been made by the digital computer. Then, discretely selected delay compensation time is set, taking 4.5 msec delay for every 60 Hz frequency gap as a unit. The second step of delay compensation is then taken to be 9 msec for every 60 Hz. As we can see in Fig. 1, a suitable delay for $NL = 320$ pc/cm^3 is between 4.5 msec and 9 msec for 26.3 MHz, and around 4.5 msec for

Fig. 15 Results of pulse forms for the decametric radiation from the galactic center obtained by the pulse period accumulation analyses for the observation period of 13380 sec (3 h 43 min). The displays are made using the same format as Fig. 6. Results for 25.5 MHz observed on July 2, 1986 (a) for 26.3 MHz observed on July 5, 1986 (b) and for 28.4 MHz observed on June 28, 1986 (c) are indicated taking a suitable delay compensation corresponding to 320 pc/cc.

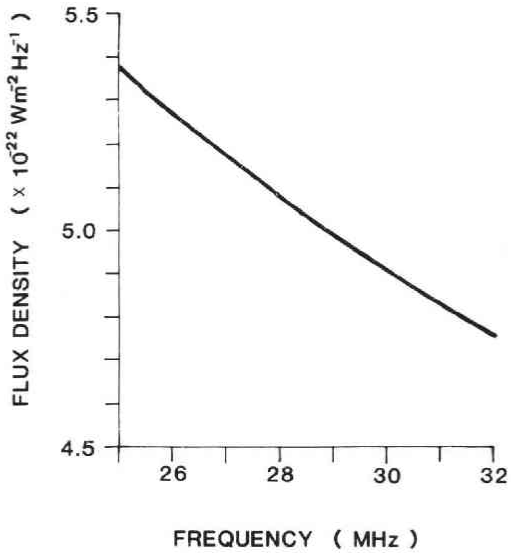

Fig. 17 Power spectra of the pulse, given in the unit of 10^{-22} Watt/m^{2}Hz, versus the observation frequency.

29.3 and 31.5 MHz for the frequency gap of 60 Hz. When we made the delay compensation by using expected delay compensation times, the pulse form becomes clearer than the case of no compensation as it can be confirmed in the results given in Fig. 18 for 26.3 MHz and Fig. 19 for 29.3 MHz. This result is strengthen when we add the results obtained by system-A as has been given in Fig. 14. The result suggests that the pulse source is located at a distance of about 9 kpc when we assume $N=0.03$/cc in the galactic space.

c) Duration

Studies on the search for the pulsating components started in May 1983 (see Table 1). The observations in 1984 and in a part of 1985 were made using the system-A (see Secs 2 and 5) and the data handling in this period was concentrated to the Fourier analyses seeking for the pulsating components and the possible pulse period.

Fourier analyses show that there were pulsating components that were dominated in a period range from 220 msec to 250 msec (see Sec 5). Though the actual period of the pulse is disclosed to be 421.60 msec, by the analyses of the pulse period accumulation method for the data obtained in 1985 and 1986, the investigation indicated that the period in a range from 220 msec to 250 msec are dominated because the pulse consists of two

Fig. 18 Pulse form obtained by the pulse accumulation analyses during the observation period of 13380 sec (3 h 43 min) for the observation data at 26.3 MHz observed on July 5, 1986. The displays made for the three dispersion compensation times as 0 msec for 60 Hz gap (a), 4.5 msec for 60 Hz gap (b) and 9 msec for 60 Hz gap (c). The results show the best wave form can be obtained at $D=9$ msec/60 Hz indicating the source is located close to 9 kpc for $N=0.03$/cc in the galactic space.

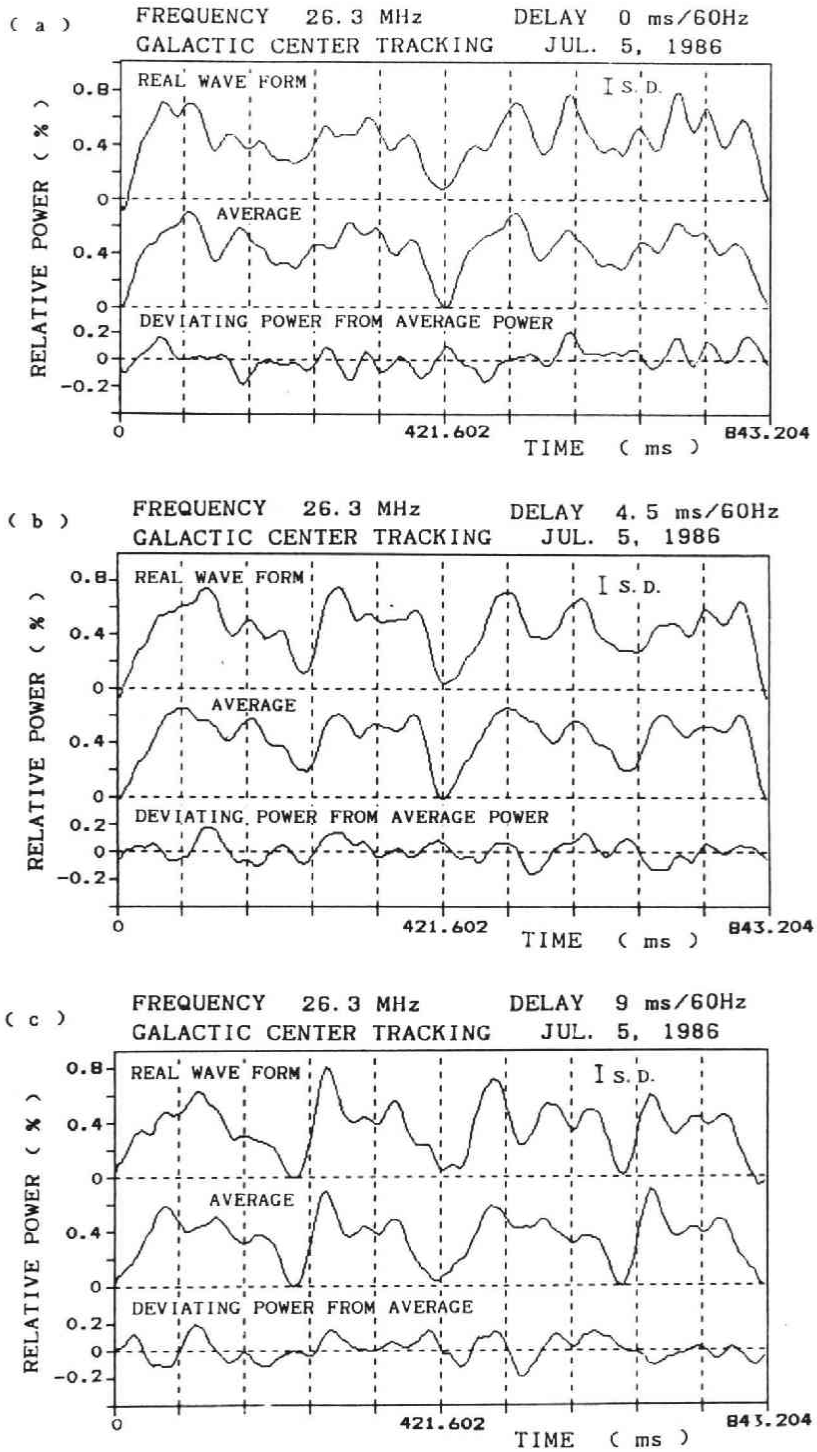
(a)
FREQUENCY 26.3 MHz DELAY 0 ms/60Hz
GALACTIC CENTER TRACKING JUL. 5, 1986
REAL WAVE FORM
I S.D.
AVERAGE
DEVIATING POWER FROM AVERAGE POWER
RELATIVE POWER (%)
0.8
0.4
0
0.4
0
0.2
0
-0.2
0
421.602
843.204
TIME (ms)
(b)
FREQUENCY 26.3 MHz DELAY 4.5 ms/60Hz
GALACTIC CENTER TRACKING JUL. 5, 1986
REAL WAVE FORM
I S.D.
AVERAGE
DEVIATING POWER FROM AVERAGE POWER
RELATIVE POWER (%)
0.8
0.4
0
0.4
0
0.2
0
-0.2
0
421.602
843.204
TIME (ms)
(c)
FREQUENCY 26.3 MHz DELAY 9 ms/60Hz
GALACTIC CENTER TRACKING JUL. 5, 1986
REAL WAVE FORM
I S.D.
AVERAGE
DEVIATING POWER FROM AVERAGE
RELATIVE POWER (%)
0.8
0.4
0
0.4
0
0.2
0
-0.2
0
421.602
843.204
TIME (ms)

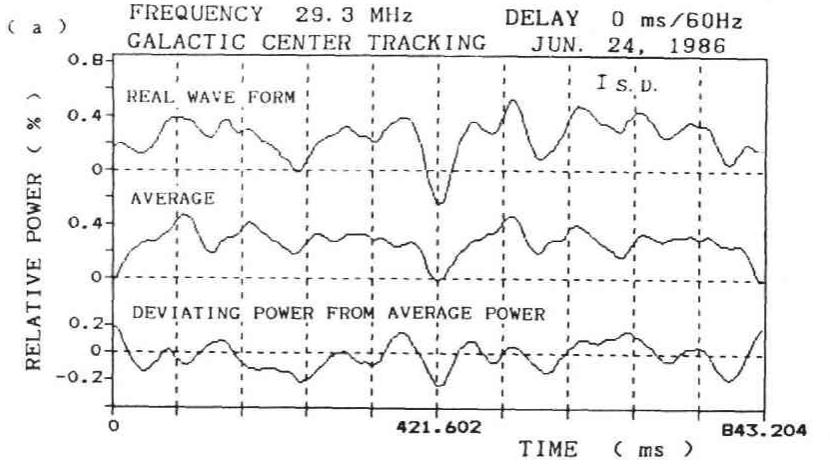
(a)
FREQUENCY 29.3 MHz
DELAY 0 ms/60Hz
GALACTIC CENTER TRACKING
JUN. 24, 1986
I S.D.
REAL WAVE FORM
AVERAGE
DEVIATING POWER FROM AVERAGE POWER
RELATIVE POWER (%)
0.8
0.4
0
0.4
0
0.2
0
-0.2
0
421.602
843.204
TIME (ms)

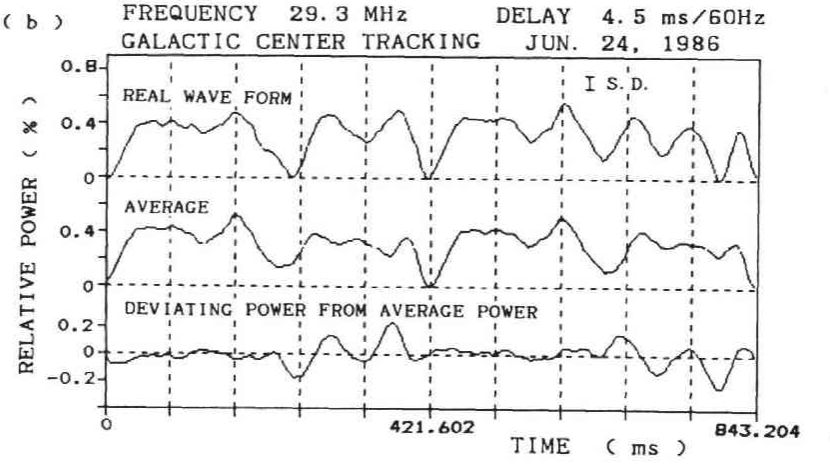
(b)
FREQUENCY 29.3 MHz
DELAY 4.5 ms/60Hz
GALACTIC CENTER TRACKING
JUN. 24, 1986
I S.D.
REAL WAVE FORM
AVERAGE
DEVIATING POWER FROM AVERAGE POWER
RELATIVE POWER (%)
0.8
0.4
0
0.4
0
0.2
0
-0.2
0
421.602
843.204
TIME (ms)

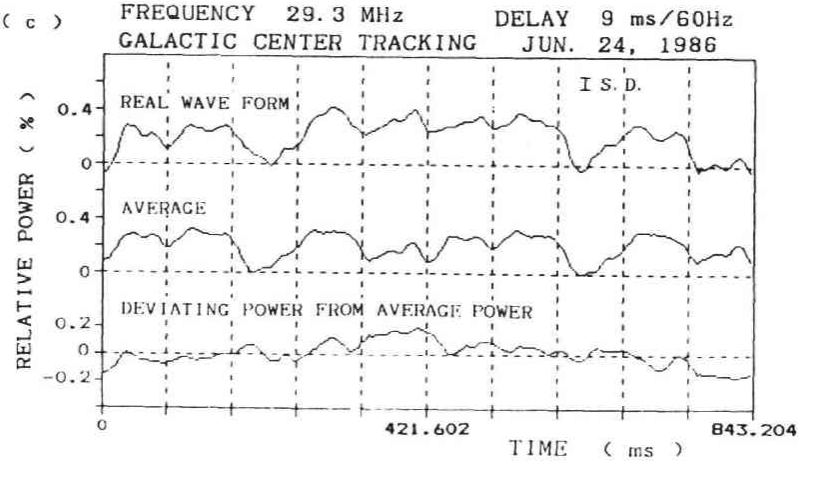
(c)
FREQUENCY 29.3 MHz
DELAY 9 ms/60Hz
GALACTIC CENTER TRACKING
JUN. 24, 1986
I S.D.
REAL WAVE FORM
AVERAGE
DEVIATING POWER FROM AVERAGE POWER
RELATIVE POWER (%)
0.4
0
0.4
0
0.2
0
-0.2
0
421.602
843.204
TIME (ms)

sub-pulses (see Sec. 5). We can, therefore, conclude that the pulse component of the present interest can be always observed whenever the Galactic center is observable.

d) Power

The pulse component has a power equivalent to $4.4\times10^{-3}\sim5.8\times10^{-3}$ of the background noise from the galactic center. The measured Galactic noise in this frequency range is in a range from 8.60×10^{-20} Watt/m^{2}Hz at 29 MHz and 1.2×10^{-19} Watt/m^{2}Hz at 25.5 MHz. The source power of the pulse component is then estimated, on the basis of the observed spectrum level which shows 5.3×10^{-22} Watt/m^{2}Hz at 25.5 MHz and 5.0×10^{-22} Watt/m^{2}Hz at 29.5 MHz (see Fig. 17). Assuming that the source is located at the distance of 9 kpc, the total power within a 10 MHz range from 25.5 to 35.5 MHz is then 5.1×10^{34} erg/sec ; this value is almost 10 times larger than the total power of the present solar radiation. Considering the evidence that the main portion of solar radiation is expanded within 10^{15}-10^{16} Hz, the power of the decametric pulse of the present study is very unusual. That is, because the power of 10 L$\odot$ is confined within a band width of 10^7 Hz, spectral density of the pulse component is about 10^{27} erg/Hz while solar radiation has spectral density of about 2×10^{17} erg/Hz. Thus it can be concluded that unusually high power is being radiated in the form of non-thermal emissions in the decametric wavelength range with the pulse period of 421.60 msec.

7. Possible Cause : Super Black Hole

7.1 *Black Hole Hypothesis*

Considering all of the evidences of the observed pulses with a period at 421.60 msec which have continued ever since the discovery, it is concluded that the radio source stems from a very compact rotating object which is at the Galactic center. Decametric radiation from plasma in its usual state shows that the magnetic field intensity corresponding to this frequency range is within a field strength range from 1 to 10 gauss. These values of the magnetic field intensity are well observed near regular stars such as the sun or near planets such as Jupiter. These objects are, however, not candidate sources of the present decametric radiation because such objects like regular stars or planets cannot emit a power corresponding to the total radiation power from a regular star within a narrow band width in decametric wavelengths. If we consider decametric emissions from the usual plasma state, a source which can provide radiations of the solar luminosity within the decametric wavelength range should have a volume that is 10^{14} times larger than the Jovian plasmasphere ; i.e., we should consider a region with a diameter of 10 AU filled with super thermal electrons contained by a magnetic field with an intensity around 10 gauss. However, the pulsation period at 421.60 msec shows that the radius of a rotating source should be less than 2×10^4 km.

Fig. 19 Same with Fig. 18, for the case of the observation at 29.3 MHz made on June 24, 1986. The dispersion compensation time D is selected at 0 msec for 60 Hz gap (a), 4.5 msec for 60 Hz gap (b) and 9 msec for 60 Hz gap (c). The results show that the most clear wave form can be obtained for the case of 4.5 msec for 60 Hz gap ; again the results are consistent with that given in Fig. 14 (30 Hz gap in Fig. 14).

To solve this discrepancy problem, we should invoke a very unusual object. We, therefore, propose that the pulsating component is coming from a region very close to a super black hole which is rotating with the period near 421.60 msec. Localized source regions in the rotating magnetic field close to the surface of the black hole may be responsible for the periodicity of the pulsating components.

To emit the very high power containing energy of about 10 L⊙ within the decametric frequency range, we should have very dense and sometimes intense magnetic fields ; this necessarily results in a very high emission frequency f_e at the source if we make observation in an inertia frame. However if the source is very close to the black hole surface the frequency decreases from f_e to the decametric frequency range when the observations are made in a local frame fixed to a region near the black hole surface with a strong gravity field, as in the following relation :

$$f = f_e \ (R_s/R)^{-1/2}, \tag{7}$$

with

$$R_s = 2GM/c^2,$$

where f_e is the electron cyclotron frequency at a distance, R, from the black hole surface and G and M are the gravitation constant and the mass of the central body, respectively. If the original radiation is generated, for example within 700 m from the edge of the black hole observed from outer space, the radiation at the local frequency ranging from 4.2×10^9 to 8.4×10^9 Hz (i.e., the local emission occurs at cm wavelengths in this case) in the inertia system, can be observed in the decametric frequency range from 20 MHz to 40 MHz in the frame of a strong gravity field. Since the frequency is conserved in a region outside the black hole surface, the emissions are always observed as decametric radiation. If the emissions take place in a layer which is much closer to the surface ; i. e. within 1 cm, the observed wavelength in a range from infrared to visible light in the local inertia system can be observed in the decametric frequency range in the region apart from the black hole surface. We may, therefore, state that the decametric emissions are providing information on the media very close to the black hole surface which could not be detectable as visible light or X-ray emissions. The decametric emissions observed outside may be the last cry from charged particles being captured by the magnetic cloud just before disappearing into the black hole.

Due to the effect of general relativity, the limiting mass, M of a super black hole corresponding to a circular length of 1.26×10^5 km is estimated to be $M = 6\times10^3$ M⊙ (i.e., 1.34×10^{37} g). From an analysis of the distribution of the velocities of clouds, a most probable mass distribution is derived by Lacy *et al*[9] which includes a central point-like mass of several times 10^6 M⊙ in addition to several times 10^6 M⊙ stars within 1 pc of the central region. However, Lacy *et al* also pointed out that due to the small number of observed clouds, their mass determination was quite uncertain. Furthermore, they have pointed out that there is the possibility of a distributed mass of about 10^7 M⊙ within a parsec of the galactic center without a central massive object. Ambiguity in determing

the central mass shows that other observational evidence is needed to provide independent information regarding the existence of the super black hole at the center of the Galaxy. In this context, our present results show that the real mass of the super black hole may be 1% of the maximum possible value inferred from the gas motion near the Galactic center.

7.2 *Possibility of the escape of the radiations*

At the place with an extremely intense gravity field, time passage is so slow that the emission frequency becomes very low and enter the decametric frequency range. Once the generated waves start to move toward the outside of space from the regions close to the black hole surface, the wave frequency f takes a condition where the frequency is lower than the local plasma frequency f_{pl} and also lower than the local electron cyclotron frequency f_{ce} with increasing distance R. The propagation of the waves in this region is possible only when the generated waves are changed to the whistler mode waves and further down to MHD mode waves. Therefore to realize this propagation the mode conversion of the waves (Oya, 1974 ; Jones, 1976 ; Budden, 1981) are essential. The detailed procedure of these conversion processes and the escape mechanism of the radiation will be given in different papers in the near future.

7.3 *Scintillation effects*

For investigating the pulsed component of the radiation, we should also consider the time varying irregularities of the plasma along the propagation path. There are a large number of obstacles, between the source and the observation points on the earth, which may produce time varying effects. These are

a) Ionospheric scintillations,
b) Interplanetary scintillations due to the solar wind,
c) Interstellar scintillations due to the stellar winds,
d) Scintillations due to the flowing plasma which contain irregularities in the accreting disc in the region near the galactic center.

All of the time varying effects caused by the flowing plasma have characteristics which could not steadily keep their effects on the pulse period because these are taking place in the frame of a changeable and turbulent state of plasma. When we accumulated the data for a long time interval, therefore, all of these scintillation effects are eliminated. The observed evidence shows that the poriod 421.6 m sec is identified for an observation interval longer than 10 minutes whereby the accuracy is increased "by an order of two" up to 421.602 msec for an observation interval longer than 200 minutes. The possible multi-path effects which will severly smear the pulse width has been discussed in the Appendix. The only solution to solve this difficulty is to select an unusualy narrow band of the receiver. The selection of a narrow band (see Sec. 2) is fortunately allowed in this case bacause the source is emitting unusually high power.

8. Conclusion

In the decametric frequency radiation from the galactic center identified within an antenna resolution angle of $\pm 15^{\circ}$ the pulsed components have been confirmed with the pulse period of 421.602 msec ± 0.007 msec ; in the frequency range from 25.5 to 32.5 MHz.

The observed pluse indicates the apparent frequency dispersion effects with the rate of 9 msec for the frequency gap of 60 Hz at 25.5 MHz and 4.5 msec for the frequency gap of 60 Hz at 31.4 MHz. This corresponds to $NL=320$ pc/cm^3 for the number densiy N and the source distance L, suggesting that the source is located at the Galactic center with a distance of about 9 kpc to 10 kpc for $N=0.03$/cc. The detected power of the pulsating components has been estimated to be about 5.3×10^{-22} Watt/m^{2}Hz at 25.5 MHz and 5.0×10^{-23} Watt/m^{2}Hz at 29.5 MHz. The total pulse power within a bandwidth of 10^7 Hz corresponds to the total power of 5.1×10^{34} erg/sec.

One of the most possible candidates to account for the source of the observed decameter pulse is a rotating black hole located at the Galactic center whose maximum size is estimated to have a circular length of 1.26×10^5 km ; the maximum total mass of 6.7×10^3 M$_\odot$ (where M$_\odot$ is the solar mass) is estimated within the Schwartzchild radius of 2×10^4 km.

The decametric pulses are most likely to be generated near the surface of the inferred black hole ; emission frequencies are considered to be shifted towards an extreme lower side dut to the intense gravity field near the black hole compared with the value observed in space with no gravitational field ; the decametric pulse radiation from the Galactic center is then concluded as the result of this extreme frequency shift.

Acknowledgements : The authors would like to express their sincere thanks to Prof. M. Oda, ISAS ; Prof. S. Hayakawa, Nagoya University ; Dr. D. Jones, British Antarctic Survey ; and Dr. E.J. Smith, JPL, NASA for their important comments on this paper.

Appendix

——Multi-Path Effects

a. *Average deviation time*

The propagation of the radio wave pulse from the galactic center are subjected to widely distributed plasma irregularities that cause smearing effects on the pulse width due to the separation of the wave energy into different paths which causes a differentiation in the arriving time of the pulse. As a first step, we select here a single refraction model of an irregularity region (I) of the plasma in between the source (S) and the observation point (O) as given in Fig. A-1. Considering small refraction angles θ_1 and θ_2 (see Fig. A-1), the time difference between two paths (between the direct path and the refracted path) is given by

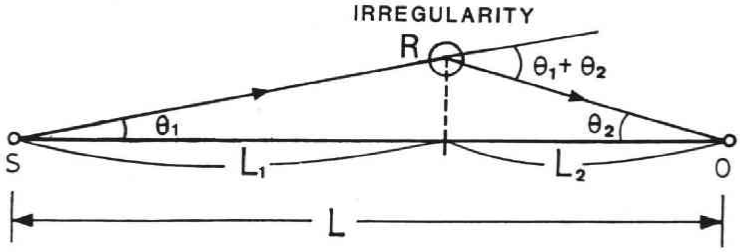

Fig. A-1 Geometry of a ray of the decametric radiation from the soure at the galactic center (S) refracting at an irregularity (R). Two rays arrive at the observation point (O) on the earth at a distance L apart from S.

$$\Delta T=\frac{1}{2C}\left(L_1\theta_1^2+L_2\theta_2^2\right), \tag{1}$$

after a simple mathematical manipulation considering

$$1-\cos\theta_i=\frac{\theta_i^2}{2}. \tag{2}$$

From the geometry given in Fig. A-1, it follows that

$$L_1\tan\theta_1=L_2\tan\theta_2. \tag{3}$$

This relation is approximated as

$$L_1\theta_1=L_2\theta_2. \tag{4}$$

Using eq (4), eq (1) is finally rewritten as

$$\Delta T=\left(\frac{L}{2C}\right)\left(\frac{L_1}{L-L_1}\right)\theta_1^2. \tag{5}$$

When we define a probability function P, throughout the galactic space to satisfy the condition of the refraction angle

$$\theta_1+\theta_2=\alpha, \tag{6}$$

for a given θ_1, as

$$P=P(\alpha, x, y, z), \tag{7}$$

where x, y, and z are given in the Cartesian co-ordinate system, the averaged deviation $\overline{\Delta T}$ is defined as

$$\overline{\Delta T}=\frac{L}{2C}\iiint_{-\infty}^{\infty}dxdydz\int_{-\pi/2}^{\pi/2}d\theta_1\,P(\alpha, x, y, z)\left|\frac{x}{L-x}\theta_1\right|, \tag{8}$$

where $x=L_1$. The relation of α, θ_1, x, y and z and the functional form of P will be described later.

b. *The probability Function P (α, x, y, z)*

We consider here a region of the plasma irregularity where the plasma density

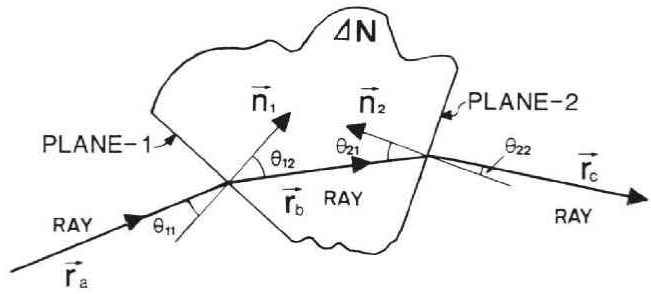

Fig. A-2 Geometry for a model irregularity consists of sharp boundaries due to the variation of the plasma density ΔN with the boundary normals $\vec{n}_1$ and $\vec{n}_2$. The ray direction vector $\vec{r}_a$ is changed to $\vec{r}_b$; and successively changes from $\vec{r}_b$ to $\vec{r}_c$ due to the refraction at the boundaries.

increases by ΔN from the background number density N, with a characteristic length l which is larger than the wevelength but shorter than the galactic propagation distance; i.e. $\lambda \ll l \ll L$, for the wavelength λ.

In Fig. A-2, the geometry for a model irregularity is shown; the structure of the irregularity is simplified as consisting of two sharp boundaries whose normal directions are given by vectors $\vec{n}_1$ and $\vec{n}_2$. Angles are defined between unit vectors indicated in Fig. A-2, as

$$\begin{aligned} \vec{r}_a \cdot \vec{n}_1 &= \cos\theta_{11}, \\ \vec{r}_b \cdot \vec{n}_1 &= \cos\theta_{12}, \\ \vec{r}_b \cdot \vec{n}_2 &= \cos(\pi - \theta_{21}), \end{aligned} \tag{9}$$

and

$$\vec{r}_c \cdot \vec{n}_2 = \cos(\pi - \theta_{22}).$$

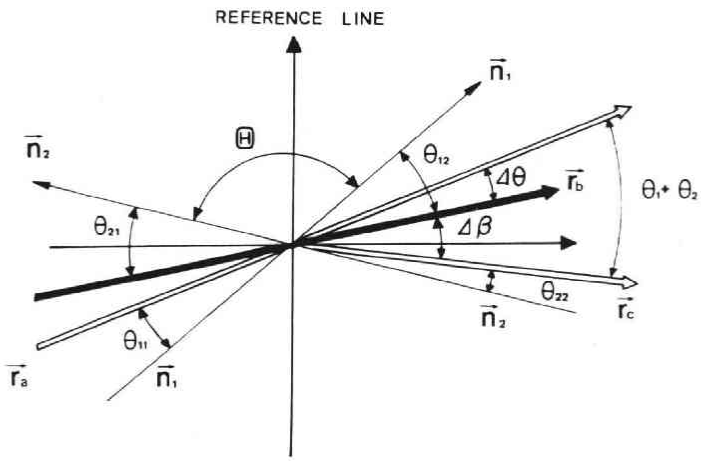

Fig. A-3 Relation of vectors $\vec{n}_1$, $\vec{n}_2$, $\vec{r}_a$, $\vec{r}_b$ and $\vec{r}_c$.

To see the relationships of vectors defined in Fig. A-2, all of the related vectors are overlapped at a point as has been given in Fig. A-3.

Snell's law gives the following relations, as

$$\eta_1 \sin\theta_{11}=\eta_2 \sin\theta_{12}, \tag{10}$$

and

$$\eta_1 \sin\theta_{21}=\eta_2 \sin\theta_{22}, \tag{11}$$

where η_1 and η_2 are refractive indices which are defined relating to the angular frequency of the propagating electro-magnetic waves, as

$$\eta_1=\sqrt{1-aN/\omega^2}, \tag{12}$$

and

$$\eta_2=\sqrt{1-a\,(N+\Delta N)/\omega^2}, \tag{13}$$

with $a\equiv e^2/m\varepsilon_0$; e, m and ε_0 are electron charge, electron mass and the dielecric constant in the rationalized unit system, respectively.

When the angle Θ is defined as

$$\vec{n}_1\cdot\vec{n}_2=\cos\Theta, \tag{14}$$

it follows that

$$\theta_{12}-\theta_{21}+\Theta=\pi, \tag{15}$$

and

$$\theta_{11}-\theta_{22}+\alpha+\Theta=\pi. \tag{16}$$

Considering $aN/\omega^2\ll 1$, it follows from eqs (10), (12) and (13), that

$$\theta_{12}=\theta_{11}+\frac{a\,\Delta N}{2\omega^2}\tan\theta_{11}, \tag{17}$$

and also from eqs (11) with eqs (12) and (13), it follows that

$$\tan(\Theta+\theta_{11})=\frac{2\omega^2}{a\,\Delta N}\left(\frac{a\,\Delta N}{2\omega^2}\tan\theta_{11}-\alpha\right). \tag{18}$$

For a given refraction condition, i.e. with fixed α value, and also for given conditions of the irregularity, the allowance range of the angle between $\theta_{11}-\frac{d\theta_{11}}{2}$ and $\theta_{11}+\frac{d\theta_{11}}{2}$ with an angle width of $d\theta_{11}$ is existing for a wave packet with a frequency band of $d\omega$, around the incident angle θ_{11}, as

$$d\theta_{11}=\frac{1}{\tan\theta_{11}}\cdot\frac{d\omega}{\omega}. \tag{19}$$

This relation can easily be obtained from eq (18) by differentiating both sides of eq (18) taking α and Θ, as constant values.

We assume, here, that the density change ΔN takes place with the Gausian probability function with the dispersion, as

$$P(\Delta N)=\frac{1}{\sqrt{\pi}}\exp\left(-\left(\frac{\Delta N}{\sigma}\right)^2\right). \tag{20}$$

In galactic space, there is no specially selected direction for the formation of the boundary normal of the irregularity region ; i.e., the probability to make θ_{11} angle enter into the angle range from θ_{11} to $\theta_{11}+d\theta_{11}$ is given by

$$P(\theta_{11})=\frac{d\theta_{11}^2}{4\pi}. \tag{21}$$

The boundary normal of the second boundary (see Fig. A-2) of the irregularity region has an important role for the reception of the signal at the observation point (O). To satisfy this reception condition, the relation given by eq (16) should hold. From eq (17), considering the relations of angles given in Fig. A-3, we can express as

$$\Delta\theta=\frac{a\,\Delta N}{2\omega^2}\tan\theta_{11}. \tag{22}$$

From eq (11), we can write

$$\left\{1-\frac{a(N+\Delta N)}{2\omega^2}\right\}\sin\theta_{21}=\left(1-\frac{aN}{2\omega^2}\right)\sin(\theta_{21}-\Delta\beta), \tag{23}$$

for $\Delta\beta$ which is also defined in Fig. A-3. From the definition

$$\Delta\theta+\Delta\beta=\theta_1+\theta_2\ (\equiv\alpha), \tag{24}$$

and from eq (23)

$$\Delta\beta=\frac{a\,\Delta N}{2\omega^2}\tan\theta_{21}. \tag{25}$$

We can finally write α as

$$\alpha=\frac{a\,\Delta N}{\omega^2}\tan\theta_{11}. \tag{26}$$

From eq (4) α can be written in another form, as

$$\alpha=\frac{L}{L-L_1}\theta_1. \tag{27}$$

Substituting eq (27) into eq (26), we can rewrite, as

$$\tan\theta_{11}=\frac{\omega^2}{a\,\Delta N}\cdot\frac{L}{L-L_1}\theta_1. \tag{28}$$

For the relation between two boundary normals $\vec{n}_1$ and $\vec{n}_2$, two extreme cases can be considered. The first is the case where the relation of two boundary normals is fixed, as were the cases where we selected sphere shaped irregularity or slab-shape irregularity. The second is the case where the boundary normal is independent between these two special cases.

We call here the first case "simply-shaped irregularity" and the second case "complex irregularity". We will discuss here the spherical irregularity as an example case of the simply shaped irregularity.

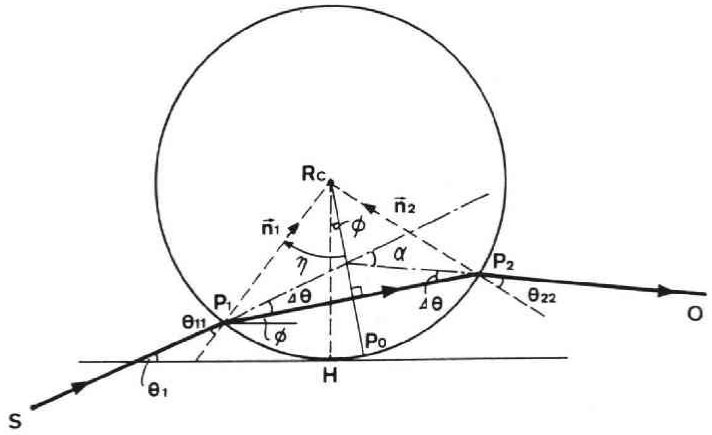

Fig. A-4 Geometry for the spherical irregularity model whose center is at Rc. All other points, vectors and anyles are consistently used in Fig. A1, A2 and A3.

c. $\overline{\Delta T}$ *value for spherically shaped irregularities*

As has been given in Fig. A-4, we consider here spherically shaped irregularity. The relations for the vectors and angles given in Fig. A-2 and A-3 are used here specified for the case of the sphere model of the irregularity where the density increases by ΔN from the back ground. A ray coming from the source S encounters the irregularity at point P_1; and after making refraction, the ray hits poiot P_2. The whole geometries show a symetrical relationship with respect to the line R_cP_o, in Fig. 4, which is selected to divide the line P_1P_2 into a half length. Let the angle between the line R_cH (see Fig. A-4) and R_cP_o be ϕ, then ϕ is written as

$$\phi = \theta_2 \tag{29}$$

For the reception of the ray in the direction of O, the tilt angle η from the R_cP_o direction to give P_1 point is decided as

$$\frac{\pi}{2} - (\eta - \phi) = \theta_1 + \theta_{11}. \tag{30}$$

There is a range of η from η to $\eta + d\eta$ corresponding to the frequency difference $d\omega$ of the wave packet as

$$d\eta = -d\theta_{11}. \tag{31}$$

The rate of ray direction to enter this range from η to $\eta + d\eta$ is then given in the case of a three dimensional spherical irregularity, as

$$P(d\eta) = d\eta^2 / 4\pi. \tag{32}$$

Using the relationship given by eq (31), it follows that

$$P(d\eta) \equiv P(d\theta_{11}) = \frac{d\theta_{11}^2}{4\pi}. \tag{33}$$

Substituting eq (19), which can be used for the case of spherical irregularity, $P(d\theta_{11})$ is

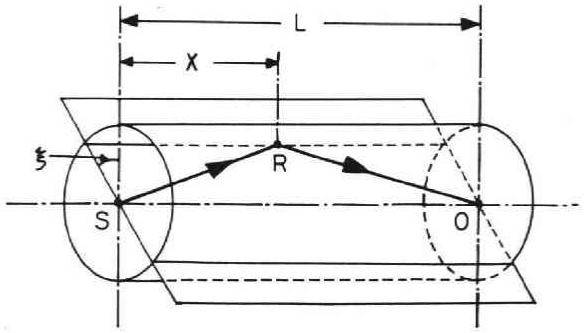

Fig. A-5 Three dimensional illustration of the geometry for the distribution of the irregularities betwwen the source (s) and the observation point (o).

rewritten as

$$P(d\theta_{11})=\frac{1}{4\pi \tan^2\theta_{11}}\left(\frac{d\omega}{\omega}\right)^2. \tag{34}$$

From eq (28), this can be further rewritten as

$$P(d\theta_{11})=\left(\frac{1}{4\pi}\right)\left(\frac{a\ \Delta N}{\omega^2}\right)\left(\frac{L-L_1}{L}\right)^2\cdot\left(\frac{1}{\theta_1^2}\right)\left(\frac{d\omega}{\omega}\right)^2. \tag{35}$$

Let's here assume that there are K (number) of irregularities distributed homogeneously within a volume of L^3. In this case, the number dn of the irregularity within a small volume at $(x,\ \theta_1,\ \xi)$ where ξ is an angle measured in the cylindrical coordinate system as given in Fig. A-5, as

$$dn=(K/L^3)\ (x\ \tan\theta_1)^2\ d\theta_1 d\xi dx. \tag{36}$$

From eqs (5), (8), (20), (35) and (36), $\overline{\Delta T}$ is formaly expressed taking $L_1=x$, as

$$\begin{aligned}\overline{\Delta T}=&\frac{L}{2c}\int_{-\infty}^{\infty}\frac{(\Delta N)^2}{\sqrt{\pi}}\exp\left(-\left(\frac{\Delta N}{\sigma}\right)^2\right)d(\Delta N)\ (K/L^3)\\&\cdot\int_0^L\int_{-\frac{\pi}{2}}^{\frac{\pi}{2}}\int_0^{2\pi}(x\ \tan\theta_1)^2\ dx d\theta_1 d\xi\left(\frac{a^2}{\omega^4}\right)\left(\frac{L-x}{L}\right)^2\left(\frac{x}{L-x}\right)\left(\frac{d\omega}{\omega}\right)^2.\end{aligned} \tag{37}$$

Integration of eq (37) gives the results, as

$$\overline{\Delta T}=K\left(\frac{\pi^3}{960}\right)\left(\frac{L}{c}\right)\left(\frac{\Delta\omega_p}{\omega}\right)^4\left(\frac{d\omega}{\omega}\right)^2, \tag{39}$$

where

$$(\Delta\omega_p)^2=\frac{(\Delta N)\ e^2}{m\varepsilon_0}.$$

The final result shows that the smearing of the pulse width by $\overline{\Delta T}$ is proportional to ω^{-4} and also for $(d\omega/\omega)^2$. For the observation of the pulse in the decametric frequency range which propagate through galactic space, it is essential to have receiver with an extremely narrow band.

References

Budden, K.G., 1981 : The theory of radio windows in the ionosphere and magnetosphere, J. Atom. Terr. Phys., **43**, 287-298.

Higgins, C.S. and C.A. Shain, 1954 : Observation of cosmic noise at 9.15 Mc/s, Aust. J. Phys., **8**, 460-470.

Jansky, K.G., 1933 : Electrical disturbances apparently of extraterrestrial origin, Proc. IRE, **21**, 1387-1398.

Jansky, K.G., 1935 : A note on the source of interstellar interference, Proc. IRE, **23**, 1158-1163.

Jones, D., 1976 : The second Z-propagation window, Nature, **262**, 674-675.

Lacy, J.H., F. Baas, C.H. Townes and T.R. Geballe, 1979 : Observation of the motion and distribution of the ionized gas in the central parsec of the galaxy, Ap. J. (Letters), **227**, L17-L20.

Lacy, J.H., C.H. Townes, and D.J. Hollenbach, 1982 : The nature of the central parsec of the galaxy, Ap. J., **262**, 120-134.

Lo, K.Y., and M.J. Claussen, 1983 : High-resolution observations of ionized gas in central 3 parsecs of the galaxy : possible evidence for infall, Nature, **306**, 647-651.

Moxon, L.A., 1948 : Variation of cosmic radiation with frequency, Nature, **158**, 758-759.

Oya, H., 1974 : Origin of Jovian decameter wave emissions-conversion from the electron cyclotron plasma wave to the ordinary mode electromagnetic wave, Planet. Space Sci., **22**, 687-708.

Raber, G., 1944 : Cosmic Static, Ap. J., **100**, 279-287.

Shain, C.A., 1953 : A comparison of the intensities of cosmic noise observed at 18.3 Mc/s and 100 Mc/s, Aust. J. Phys., **7**, 150-164.

Shain, C.A. and C.S. Higgins, 1953 : Observation of cosmic noise at 9.15 Mc/s, Aust. J. Phys., **7**, 130-149.